MLM-2296

MLM-2296

Mound Laboratory Activities for the Division of Physical Research: July-December 1975

May 14, 1976

NOTICE

PORTIONS OF THIS REPORT ARE ILLEGIBLE. It has been reproduced from the best available copy to permit the broadest possible availability.

Research and Development Report

MOUND LABORATORY
Miamisburg, Ohio
operated by
MONSANTO RESEARCH CORPORATION
a subsidiary of Monsanto Company
for the
UNITED STATES ENERGY RESEARCH AND DEVELOPMENT ADMINISTRATION
U. S. Government Contract No. E-33-1-GEN-53

Monsanto

DISCLAIMER

MLM-2296
TID-4500
Distribution Categories UC-4 and 22

Mound Laboratory Activities for the Division of Physical Research: July-December 1975

Issued: May 14, 1976

NOTICE

PRINTED IN THE UNITED STATES OF AMERICA

Available from
National Technical Information Service
U. S. Department of Commerce
5285 Port Royal Road
Springfield, Virginia 22161
Price: Printed Copy $4.00; Microfiche $2.25

MONSANTO RESEARCH CORPORATION
A Subsidiary of Monsanto Company

MOUND LABORATORY
Miamisburg, Ohio 45342
operated for

UNITED STATES ENERGY RESEARCH AND DEVELOPMENT ADMINISTRATION
U. S. Government Contract No. E-33-1-GEN-53

NOTICE
This report was prepared as an account of work sponsored by the United States Government. Neither the United States nor the United States Energy Research and Development Administration, nor any of their employees, nor any of their contractors, subcontractors, or their employees, makes any warranty, express or implied, or assumes any legal liability or responsibility for the accuracy, completeness or usefulness of any information, apparatus, product or process disclosed, or represents that its use would not infringe privately owned rights.

Foreword

The Mound Laboratory Activities for the Division of Physical Research report, issued semiannually, replaces the previously published quarterly reports, Stable Gaseous Isotope Separation and Purification Report and the Mound Laboratory Chemistry and Physics Progress Report. Under the sponsorship of the ERDA Division of Physical Research, Mound is responsible for furnishing material to be used in the physical sciences to further the progress of science and technology in the public interest. Additional research activities of related interest under the sponsorship of the Division of Military Applications are also published in this report.

This report is submitted by W. T. Cave, Director of Nuclear Operations, and R. E. Vallee, Manager of Technology Applications and Development, from contributions prepared by W. M. Rutherford, Science Fellow (Thermal Diffusion); W. L. Taylor, Science Fellow (Gas Dynamics and Cryogenics); G. L. Silver, Senior Research Specialist (Separation Chemistry); R. J. De Sando, Advanced Development Manager; and from members of the Isotope Separation Section: R. A. Schwind, Isotope Separation Manager; E. Michaels, Leader, Isotope Separations Development; W. J. Roos, Leader Stable Isotopes Production; B. E. Jepson, Leader, Metal Isotope Separation; R. M. Watrous, Leader, Radioisotopes Separation; and V. L. Avona, Leader, Stable Isotope Sales.

These reports are not intended to constitute publication in any sense of the word. Final results will either be submitted for publication in regular professional journals or be published in the form of MLM topical reports.

R. E. Fitzharris, Editor

Table of Contents

The operating pressure for the four column, helium thermal diffusion system has been raised from 2750 torr to 3235 torr. This change has resulted in about a 23% increase in the rate of production.

Transport calculations have shown that a 3-1 column configuration gives optimum results in enriching relatively low concentrations of helium-3 to product grade and in enriching helium-4, high concentrations, to 99.9% helium-4 or greater. When the helium-3 concentration is 80% or greater, a 2-2 configuration gives about a 50% higher product rate than the 3-1 configuration. The helium thermal diffusion system is being modified to take advantage of these characteristics and will be simply convertible from a 3-1 to a 2-2 configuration, that is, convertible from producing product helium-3 to stripping helium-4 out of the stored gas to simplify storage.

Two batches of 99% krypton-78 have been produced. Additional intermediate material is being produced for enrichment to 90% and 99% krypton-78.

Intermediate material is being produced for subsequent enrichment of krypton-83 to greater than 70%. Two batches of greater than 70% krypton-83 have been produced, and a third batch is approaching product concentration.

The thermal diffusion cascade formerly used to produce enriched krypton-82 is being converted for xenon-124 enrichment.

During this period, a third batch of aged krypton depleted in krypton-85 was produced, and processing of a fourth batch was begun.

Neon-20 and neon-22 are being enriched to product grade in a four-column system.

There were 326.3 g of oxygen-18 produced as oxygen gas by electrolysis.

During this period, progress was made in two major areas:

1. Review and updating of the detailed design.
2. Start of project construction.

Start up is planned for mid-calendar year 1976.

During this period, three thermal diffusion systems produced the following quantities of product: 1.4 STP liters of greater than 20% xenon-124, 0.76 STP liter of greater than 40% xenon-124, and 6 STP liters of greater than 80% xenon-136.

The purification chromatograph purified 2.8 liters of xenon, grading 20% xenon-124. Another 0.89 liter was purified, grading 40% xenon-124.

LOW TEMPERATURE RESEARCH

METAL HYDRIDE RESEARCH

SEPARATION CHEMISTRY

COMPUTER OPERATIONS IN HH-BUILDING

Introduction

The new MODCOMP computer system operating in HH-Building was developed to help satisfy the varied computer needs of programs conducted for the Division of Physical Research. The objective was to develop a single, integrated system with multiprogramming, real-time capabilities. The resulting system has been configured to support analytical instrument control, real-time data acquisition, data reduction, process monitoring and control, product inventory control, and general batch-type computations. The hardware/software components were described earlier.[1]

A room centrally located in HH-Building has been constructed to permanently house the computer system, related process I/O, and communications hardware. The system has just been moved to this location and is now operational.

Current and Recently Completed Projects

Several software projects have been developed to the point where they can be used routinely. These include a mass spectrometer program, accounting programs, and numerous batch-type computational programs.

The first real-time program to be developed was for the operation of a CEC 620 cycloidal mass spectrometer, an instrument which is used for process control analyses of samples from isotope separation systems. Hardware and software have been developed concurrently. The software includes sections for spectrometer control (not yet completed), data acquisition, data reduction, spectrum plotting, and report writing. Since all of the separation systems depend on mass analyses for control functions, this program will provide the basis for future automated process control applications. This software is still in elementary form and will undergo further development.

A second mass spectrometer control program, for the operation of a quadrupole-type instrument, is being developed. This program will be used with two current instruments: one for separations research and the other to be used as a detector in beam scattering experiments.

A point that should be emphasized is that these real-time programs are being developed in FORTRAN IV. They execute concurrently as real-time tasks, sharing common subroutines, as memory space permits.

Interactive programs have been written to help with certain accounting procedures such as aiding in the development of tabular information on product inventory levels and sales. Also near completion, is a data base program that will process all physical inventory and sales information. Data will be available on all product isotopes including inventory on hand, enrichment, selling price, etc. This information can be accessed at any time in an interactive mode. The program will also be used for the preparation of weekly and monthly reports dealing with this information.

Several FORTRAN programs have been modified for operation under the MODCOMP executive system. For example, transient cascade calculations and scattering cross section calculations are now routinely performed on the system. The IBM Scientific Subroutine package and the IBM Commercial Subroutine package have been added to the system and are available for use.

New Projects

Current plans call for further development of real-time tasks for process control as well as further development of data base programs. In particular, the mass spectrometer programs will be enhanced for more automatic operation.

A major project will be the automation of a neon separation system. This will require substantial hardware and software development and should provide the information needed for the development of other process systems.

Hardware has been acquired from MODCOMP for a remote data acquisition subsystem (REMAC) to be used in conjunction with the scattering chamber. This subsystem can be operated up to 5,000 ft from the computer and will handle all digital and analog transfers between the scattering chamber and the computer. Work is now in progress on the implementation of this system. *(R. E. Eppley)*

Isotope Separation

ARGON

The 13-column, hot wire, thermal diffusion cascade has continued to produce greater than 99.5% argon-36. Production of intermediate argon-38 was started when a sufficient inventory was built up in the system. The argon-38 concentration was approximately 6% when production was started, instead of the previously estimated value of 25%. This was done to simplify the control of product flow rates as the system is changed from one to two product streams. This intermediate argon-38 will be collected and saved for later enrichment to greater than 95%. *(G. E. Struber)*

During this period, a 19-column thermal diffusion system produced approximately 1800 STP liters of greater than 99.95% argon-40. The system was also used to perform a special argon-37 enrichment for the University of Bern, Switzerland. The argon-37 enrichment factor in the enriched sample was 90. *(W. J. Roos)*

CARBON

^{13}C Produced (g)	Product	^{13}C Grading (%)
210.8	CO_2	99
88	CO_2	90
13.7	CH_4	97
264.156	CH_4	90
13.4	$BaCO_3$	97
405.0	$BaCO_3$	90
20.1	C	97
51.0	C	90

Also during this period, a 115 STP-liter batch of methane with a carbon-13 concentration of greater than 99% was produced. Processing of a second batch is currently in progress. Feed material for these enrichments had carbon-13 concentrations of greater than 90%. *(W. J. Roos)*

HELIUM

A total of 2136 liters of helium, grading 99.9% helium-3, was produced. Another 263 liters of helium, grading 99.98% helium-3, was also produced.

The operating pressure of the four-column, helium thermal diffusion system has been raised from 2750 torr to 3235 torr. This change has resulted in about 23% increase in the rate of production.

Transport calculations made for the four-column, helium thermal diffusion system reveal that a 3-1 column configuration is good for enriching relatively low concentrations of helium-3 to product levels. However, a 2-2 column configuration can give about a 50% product rate increase when higher helium-3 enrichments are used for feed. Calculations were also made that show that if the top and bottom of the system in the 3-1 configuration are reversed from their present arrangement; the helium-4 content can be enriched to 99.9% helium-4 and disposed of at a very high rate. Since there is a substantial quantity of helium stored at low-to-middle enrichments of helium-3, it would be advantageous to reduce the total volume of gas stored by disposing of the helium-4 content. Therefore, design modifications are being made so that by merely flipping one, four-pole, double-throw switch and turning a few valves; the system can be operated to enrich and store helium-3 of any concentration or to enrich and dispose of helium-4. A useful by-product of helium-4 disposal is the raffinate of this process, which is enriched in helium-3. This raffinate can be immediately reused as feed for helium-3 enrichment. *(J. C. Liner)*

KRYPTON

The 19-column thermal diffusion cascade has been modified by isolating the top column from the remainder of the cascade. This top column has been used to produce two batches of greater than 99% krypton-78 from previously enriched material with 90 to 96% krypton-78. The remainder of the system continued to produce intermediate krypton-78 for later enrichment to 90% and 99%.

The nine-column, five-stage thermal diffusion cascade has continued to produce intermediate material for subsequent enrichment of krypton-83 to greater than 70%.

The 10-column, nine-stage cascade has produced two batches of greater than 70% krypton-83. The system has been refilled and is currently enriching another batch of krypton-83.

The 19-column, seven-stage thermal diffusion cascade formerly used for krypton-80 and krypton-82 production has ceased producing these materials. It is presently undergoing column performance evaluations prior to beginning enrichment of light xenon isotopes.

During this period, the third batch of aged krypton in which the krypton-85 was depleted by a factor of greater than 1000 was produced. Processing of a fourth batch was begun. *(G. E. Stuber and W. J. Roos)*

NEON

Quantities of neon-20 and neon-22 are available that do not meet product specifications (namely 99.95% neon-20, 99.9% neon-22, 99.5% total neon). These materials are being upgraded to product quality in a system consisting of four, hot-wire, thermal diffusion columns in series with an intermediate reservoir connected to the system by means of a circulating loop. The system and reservoir are filled with one of the isotopes that subsequently has its chemical and isotopic purities increased as contaminants, and other isotopes are transported out of the reservoir to the ends of the system. *(G. E. Stuber)*

OXYGEN

There were 326.3 g of oxygen-18 produced as oxygen gas by electrolysis. *(J. C. Liner)*

SULFUR

The detailed design for the sulfur-34 project has been reviewed and updated, and construction is well underway.

In the review and updating of the detailed design, five major areas were involved:

1. Overall process absorber
2. Materials of construction
3. Reboiler-desorber efficiency
4. Caustic delivery system
5. Oxidation prevention

In the overall process absorber, SO_2 (97% process recycle, 3% fresh feed) is absorbed in 3M NaOH to make an $NaHSO_3$ solution for delivery to the isotope exchange columns. The final design for the absorber consists of a two-stage packed bed with interstage cooling. This design was decided upon because of heat transfer considerations; if performed in a single-stage packed bed, the absorption process could release enough heat to bring the temperature of $NaHSO_3$ solution almost to boiling; and heat transfer for interstage cooling is approximately 40 times more effective than heat transfer to a packed bed.

A corrosion testing and a heat transfer study caused two revisions to be made in the materials of construction for the sulfur system. First, Hastelloy B was found to be attacked in areas of moderate-to-high SO_2 concentration; as a result, ceramic packing and Teflon internals have been substituted for Hastelloy B in areas of moderate SO_2 concentrations. Second, a heat transfer analysis of the desorber revealed that Kynar, with a temperature limit of 350°F, should be substituted for polypropylene, with a temperature limit of 250°F.

For the reboiler-desorber units in the sulfur system, some questions were raised regarding their ability to reflux all of the concentrated $^{34}SO_2$ back to the isotope columns. However, a mass transfer analysis of each unit showed that mole fractions of less than 10^{-10} may be attainable in the reboiler waste streams. This would result in decreases of less than 0.01% of normal production rates from losses through the reboiler waste streams.

Originally, the caustic delivery system was designed to handle 3M NaOH directly from a vendor. Since a savings of approximately $10 per gram of ^{34}S will result from buying 12M (50%) caustic and diluting to 3M in-line, a system has been designed to do this.

A possible oxidation problem can exist in the isotope exchange system if oxygen is introduced; SO_2 can oxidize to SO_3 which does not participate in the isotope exchange. Consequently, nitrogen sparging systems have been included in the NaOH and H_2SO_4 storage tanks to prevent the introduction of oxygen.

During this period, actual project construction was started and is now approximately 50% complete. The major items that have been installed are the outside storage tanks, all of the system pumps, and much of the system piping. Presently, the isotope exchange columns are being installed, and soon the reboiler

desorbers will be installed. The construction should be completed in time for start up in mid-calendar year 1976. *(R. F. Cmar)*

XENON

During this period, a 19-column thermal diffusion system produced approximately 0.760 STP liter of greater than 40% xenon-124. A 24-column thermal diffusion system produced approximately 1.4 STP liters of greater than 20% xenon-124.

An eight-column, hot wire, thermal diffusion system produced approximately 6 STP liters of greater than 80% xenon-136.

The purification chromatograph purified about 2.8 liters of xenon, grading 20% xenon-124. Another 0.89 liter was purified, grading 40% xenon-124. *(J. C. Liner)*

Low Temperature Research

BORON STUDY

Several years ago, samples of cubic boron were produced in a plasma torch at Mound Laboratory. This new form of boron was one of several crystal structures produced by dropping very pure boron powder through the torch. The lattice parameters and crystal structures for these forms have been reported previously.[2] The cubic form is of particular interest because of a prediction[3] that if such a form were found, and if it were metallic, there would be a good chance it would be superconducting with a reasonably high transition temperature.

The cubic crystals are very small, averaging about 0.05 mm on a side. The first test for superconductivity was made by putting about 60 of the crystals in a specially-made secondary coil of a susceptibility bridge. The coil shown in Figure 1 was composed of 1200 turns of No. 55 (13μm diam) copper wire wound on a stainless tube with a nine mil i.d. A piece of pure indium wire was rolled between two glass plates down to a diameter of about three mils and was measured in the coil system. The superconducting transition at 3.4 K was easily detected by the Cryotronics susceptibility bridge. The boron sample was then measured down to 0.4 K, and no superconducting transition was seen. These measurements were done in collaboration with W. R. Wilkes.

Then, a pair of fine tweezers was electrically wired to measure the resistance of individual crystals at 300 K and 77 K. It was found the cubic boron was semiconducting with a room temperature resistivity of ~4 x 10^3 Ωcm. We also obtained some samples of cubic YB_{70} through MRC in Everett, Massachusetts, which is also semiconducting with a room temperature resistivity of 2 x 10^4 Ωcm. At this point, the search for superconductivity in these materials was temporarily suspended.

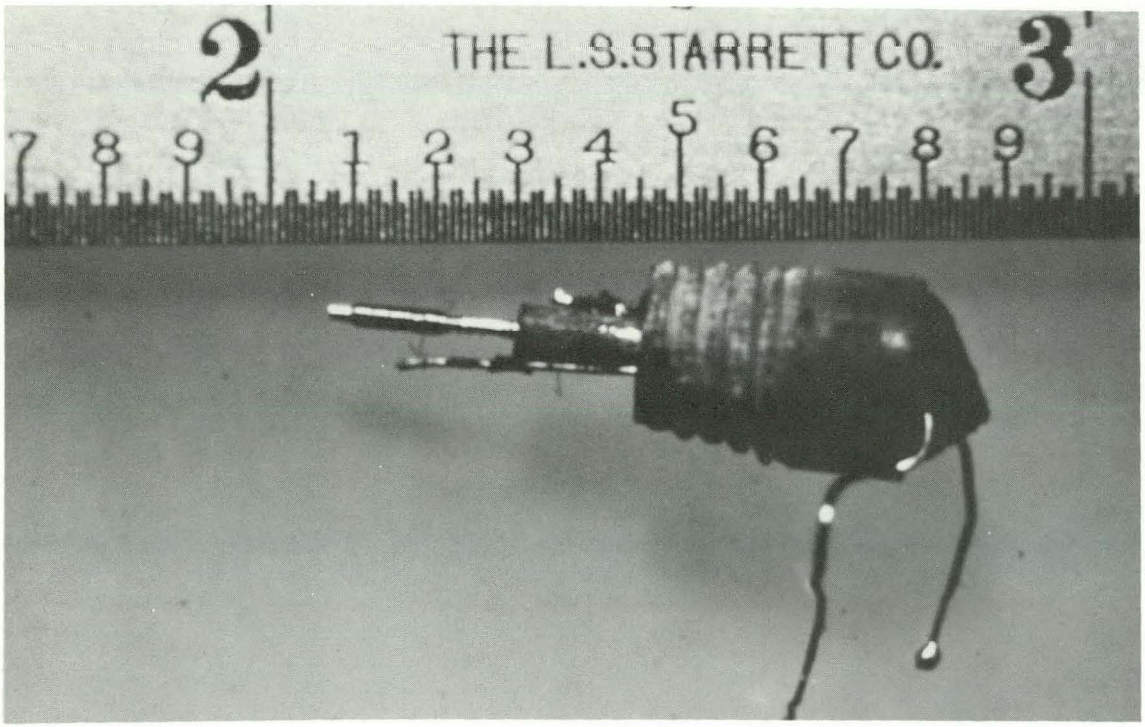

751195

FIGURE 1 - Specially-made secondary coil.

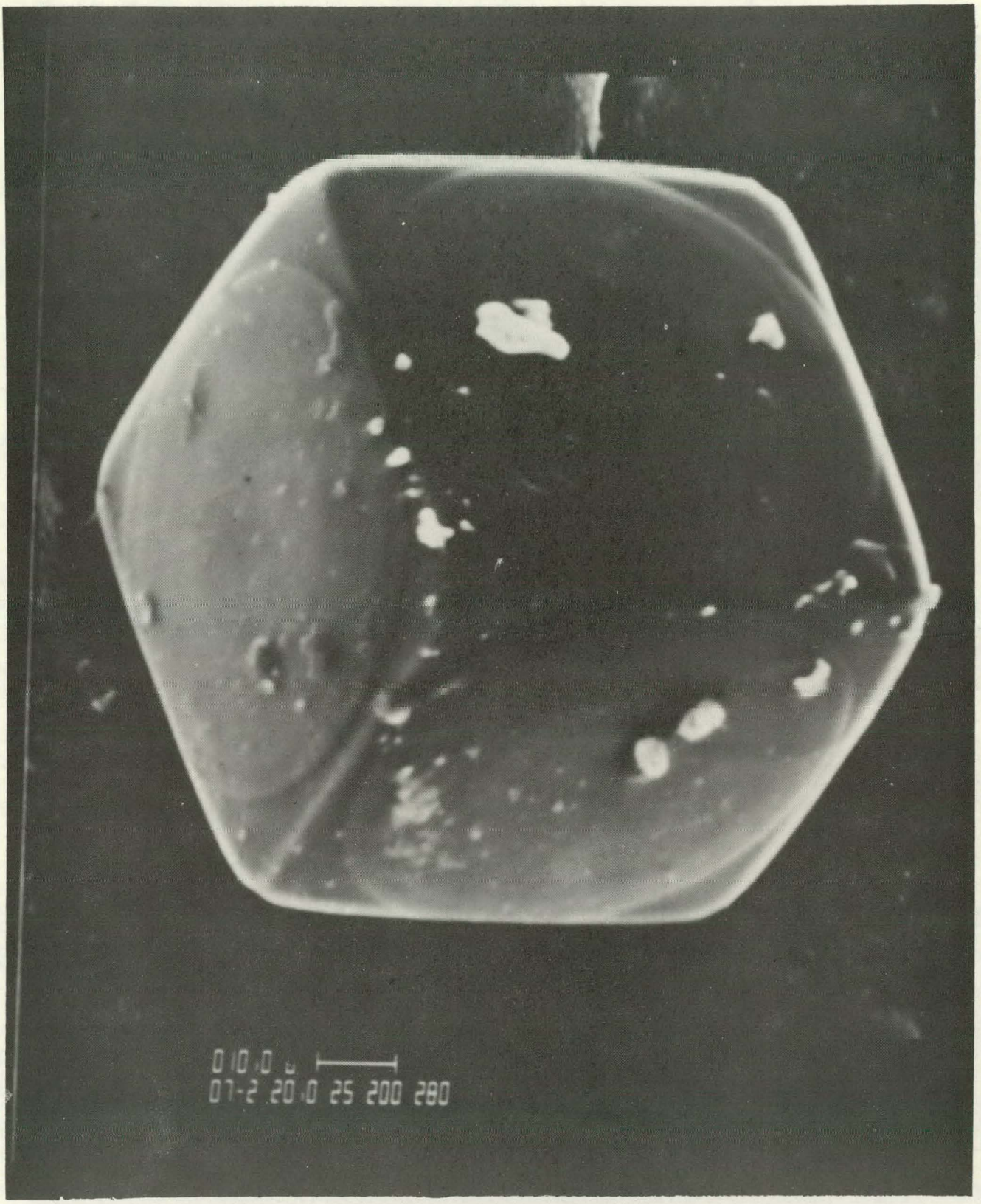

FIGURE 2 - Photomicrograph of large boron cube.

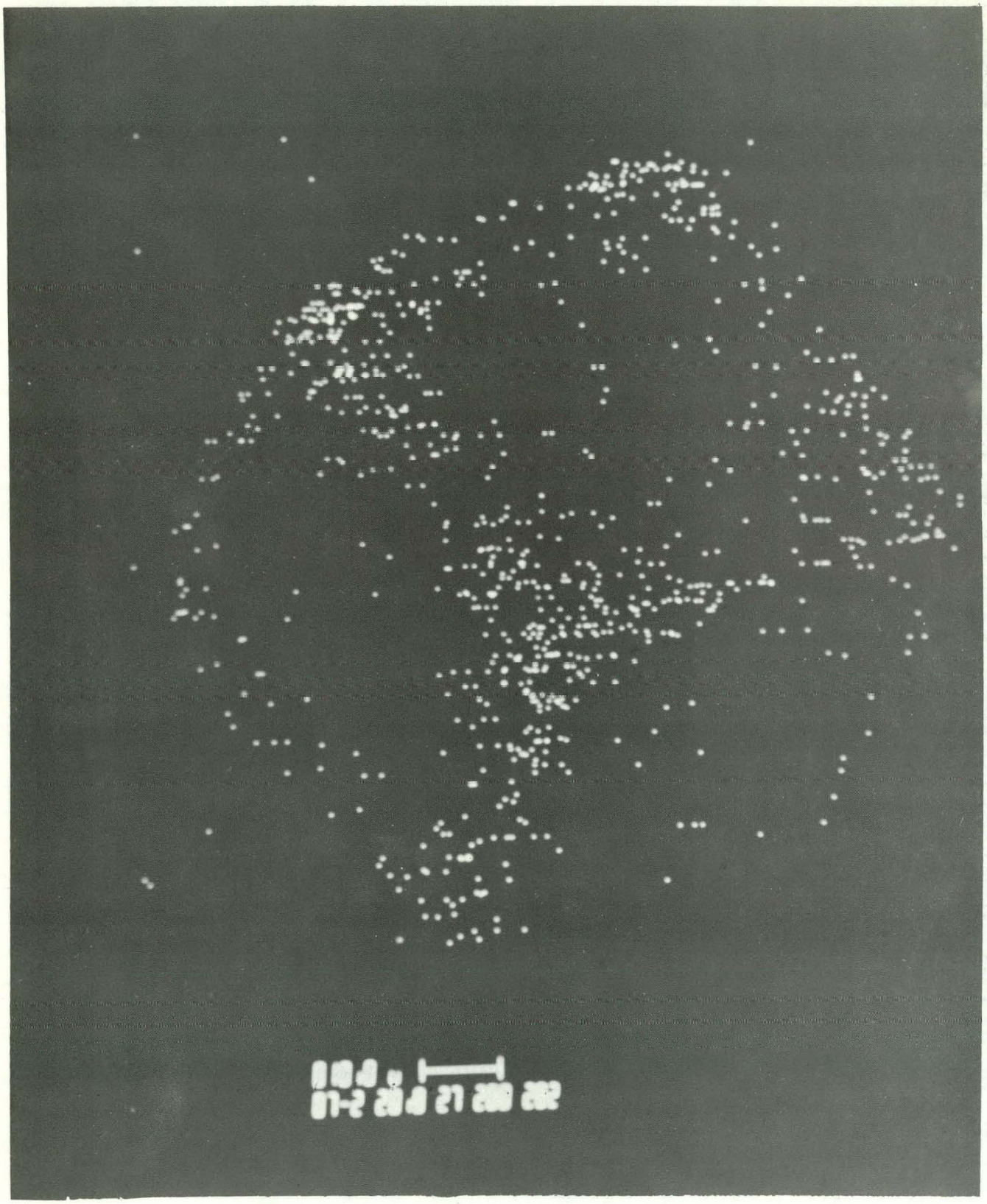

751192

FIGURE 3 - X-ray fluorescence scan for calcium.

751194

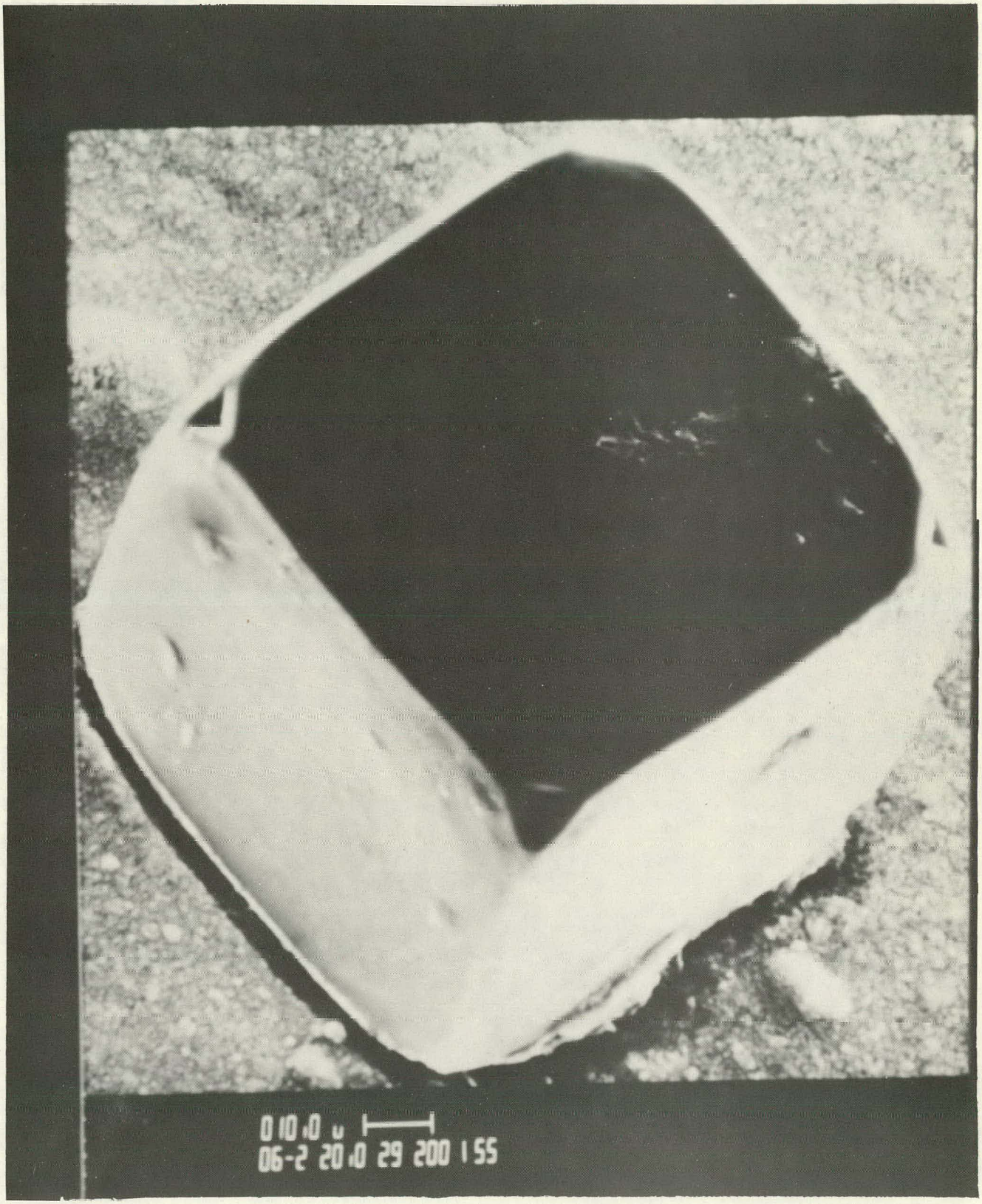

FIGURE 4 - Impurity scan for Cube No. 2.

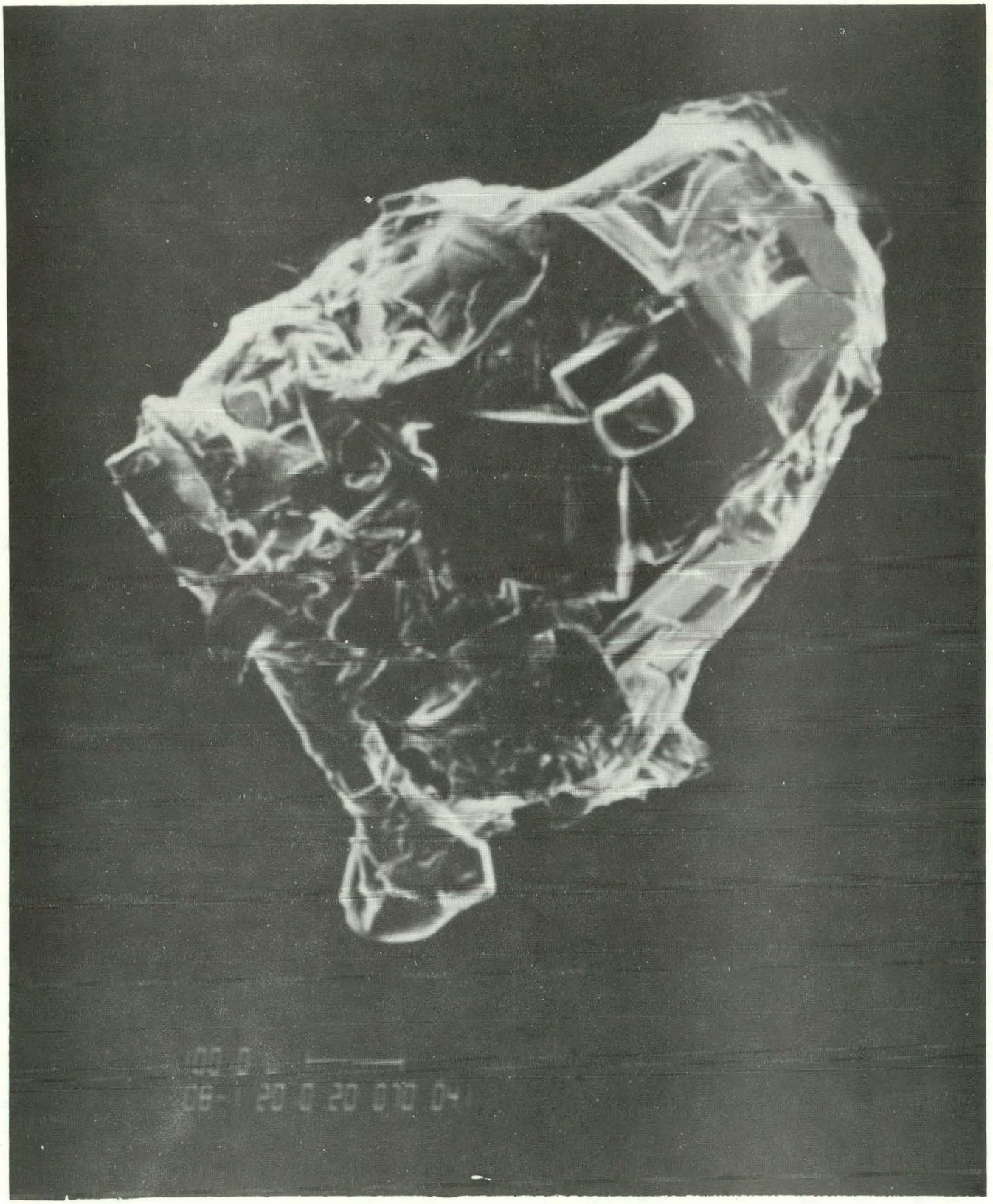

751193

FIGURE 5 - Photomicrograph of YB_{70} sample.

This past summer, at the ERDA Superconductivity Information Meeting, I met Dr. Don Gubser of the Naval Research Laboratory. Dr. Gubser has a facility to look for superconductivity at pressures up to 100 kbars, and there was a chance that these pressures might produce metallic behavior in the boron or YB_{70}.

Thus, samples of cubic boron and YB_{70} were characterized at Mound Laboratory and taken to the Naval Research Laboratory for the superconductivity measurement. There, the measurements were taken with Don Gubser in his laboratory. An impurity analysis was performed by Ron Zielinski on the scanning electron microscope. A photomicrograph of a large boron cube is shown in Figure 2. The nearly perfect growth rings are quite out of the ordinary and would be of interest to study in themselves. It was found that the principal impurity in this cube was Ca, as is shown in the scan of the Ca x-ray fluorescence in Figure 3. It is interesting to note, that the Ca concentration is much greater near the cube edges than inside the circles. This segregation remained true after several ion etches. This cube, labeled No. 1, is being saved for further study. The characterization of the cube is shown in Table 1. The density and lattice parameter are common for all the cubes, whereas the impurities and resistivity apply to Cube No. 1.

The lattice parameters were determined by Don Sullenger. Impurity scans were taken for two other cubes which are being used in the superconductivity experiment. Cube No. 2 is shown in Figure 4, and the impurities for all three cubes are given in Table 2. It was first through that the Ca impurity was what stabilized the cubic phase. The absence of Ca in Cube No. 2 indicates that the cubic form seems to be independent of the calcium. The stabilizing mechanism for these metastable forms of boron needs more study.

A sample of YB_{70} is shown in Figure 5, and the physical characteristics are shown in Table 3. It is seen that these materials have a very large lattice parameter and a very open lattice. In the case of the YB_{70}, the yttrium occupies holes in the boron lattice. It was assumed that this material would have superconducting properties similar to the cubic boron.

The apparatus at the Naval Research Laboratory, which is used to obtain very high pressures at very low temperatures, is a diamond anvil press mounted on a ^3He-^4He dilution refrigerator. The system has been described in detail in two Naval Research Laboratory publications.[4,5] The

Table 1

CHARACTERIZATION OF BORON CUBE

Starting Material - 99.99+ B

After Quench

Density - 2.367 g/cc

Lattice Parameter - 23.472 ± 0.006 Å

Impurities (%) Ca - 0.41
Al - 0.23
Si - 0.17
Ni - 0.08
Cu - 0.05
Fe - 0.04

Electrical Resistivity (Ωcm)

300 K - 4×10^3

77 K - 10^6

Table 2

BORON CUBES

Impurities (%)	No. 1	No. 2	No. 3
Ca	0.41	0.00	0.20
Al	0.23	0.21	0.00
Si	0.17	0.21	0.13
Ni	0.08	0.10	0.15
Cu	0.05	0.07	0.04
Fe	0.04	0.04	0.04

Table 3

CHARACTERIZATION OF YB_{70}

Lattice Parameter - 23.38 ± 0.06 Å

Impurities (%) Al 0.06
Ca 0.05
Cu 0.04
Si 0.04
Fe 0.03
Ti 0.03

Electrical Resistivity (Ωcm)

300 K - ~2×10^4

77 K - ~10^7

dilution refrigerator reaches temperatures of 0.030 K by pumping the ^{3}He through a phase separated mixture of ^{3}He and ^{4}He. On the bottom of the mixing chamber, is a bellows chamber that is filled with liquid ^{4}He. The ^{4}He can be pressurized to ~25 bars before it solidifies at these low temperatures. The bellows piston presses on the top diamond in the anvil. The diamonds' points have been ground flat with a diameter of 0.5 mm. The ratio of piston-to-diamond area ratio gives a pressure multiplication of 10^4. The sample is placed in a six mil hole in a Be-Cu gasket that fits between the diamonds. Above the elastic limit of the gasket (~15 kbars), the gasket flows and then the pressure on the sample is nearly hydrostatic up to 100 kbars.

Boron Cube No. 2 was just the right size to fit in the gasket hole. The gasket was placed in the press and cooled to 0.03 K. The pressure was applied to the liquid helium in the bellows through a motor driven pressure regulator. It was the first try in an experiment to apply the pressure in a controlled way.

The detection system was a superconducting transformer linked to a SQUID (Superconducting Quantum Interference Detector). The SQUID transforms small changes in magnetic field into voltage changes that can be easily amplified and displayed. The transformer consists of two coils wound in opposition around the gasket and a single loop in the SQUID. The two coils have equal area times turns products so that external changes in field tend to cancel, whereas a field change within the inner coil will be seen. The sensitivity of the SQUID is on the order of 10^{-7} G-cm^2. Thus, when the sample goes into the superconducting state the expulsion of the earth's magnetic field should easily be seen.

In cooling the sample to 0.03 K, no transition was seen. As the pressure was applied up to 100 kbar, no transition was seen. This must be qualified in that a second phenomenon was observed. Noise was seen in the SQUID as the sample was compressed. The noise was not random but systematic in that the signal was always the same direction of the order of three or four flux jumps (2×10^{-7} G-cm) and returning to the null. On returning to the null, a heat pulse was noticed on the thermometer. Thus, a direct observation of energy storage and release in compressing the Be-Cu gasket has been made. It is possible, but not very probable, that the superconducting transition was masked by the compression noise.

When a pressure 100 kbars was reached, the sample and container were warmed to 4.0 K where the detection coil goes into the normal state. In this process, no superconducting transition was seen. A second experiment will be run with Cube No. 3.where the pressure will be run up to 100 kbars at a temperature just under 4.0 K to close the path in the P vs.T diagram. At about 4.0 K, the noise caused by compression of the gasket cannot be seen. An experiment is also planned for the YB_{70} sample. *(G. T. McConville)*

Metal Hydride Research

BAND THEORY AND ELECTRONIC STRUCTURE

The development of the self-consistent plane wave Gaussian (SCPWG) computer codes for the calculation of electronic properties of solids has continued along the lines of increased efficiency and simplified operation. An effort has been made to develop a computational package that could be used by other workers who do not have a specialized background in such calculations. For this reason, two different versions of the programs have been developed. The first version has considerably larger dimensions of variables and is intended for production runs in a batch mode of entry. The second version has minimal dimensions and prompting messages and is intended primarily for interactive runs under the CDC INTERCOM system; it is extremely useful for development of basis sets, computational parameters, and an increased understanding of the programs. Also, it can be used in a batch mode of entry if desired. A continued effort toward the documentation of these programs and their release through authorized ERDA procedures is being made. Inquiries from interested individuals concerning the status of this effort will be welcomed.

The present area of program development is to generalize the computer code, which describes the crystal symmetry, so that more complicated crystal structures can be calculated. At present, the structures that can be handled are: simple cubic, face-centered cubic, body-centered cubic, and zinc blende. Furthermore, program restrictions limit one to two types of atoms of each type per unit cell. Many of the crystal structures of the transition metals are relatively more complicated (such as body-centered tetragonal, hexagonal close-packed, etc.). Minor, but somewhat time-consuming, changes will have to be made in the computer codes to handle materials of interest. It is expected that these changes will allow one to perform calculations for systems containing up to four types of atoms and six atoms of each type per unit cell.

Concurrent with this program development, we are presently using the programs for calculation of titanium and titanium hydrides in cubic phases. This work has been hampered by several unforseen computational factors. The first of these factors relates to an initial effort to determine the computer resources necessary for large systems. We are finding that the initial estimates are not as favorable as originally thought. Earlier changes in the codes, which resulted in a significant decrease in computer time requirements have been found to be in error. Although technically correct, some code changes resulted in an intolerable decrease in computational accuracy.

It has also not been possible to improve upon the local density exchange approximation to the Hartree-Fock exchange. Earlier theories toward the reformulation of the idea of a local approximation to the Hartree-Fock exchange have not been successfully implemented into computer codes. When applied to test cases involving atoms, they were found to be unsatisfactory in reproducing Hartree-Fock results.

Efforts have also begun at Mound to perform accurate Hartree-Fock and unrestricted Hartree-Fock calculations of clusters of atoms rather than perfect crystals. Toward this end, we have obtained a modified version of an earlier program named Gaussian 70, which is an ab initio, self-consistent field, molecular-orbital program for small-to-medium sized molecules; it is expected that this program will enable us to make calculations of hydrogen atoms and molecules within clusters of metal atoms. With this capability, one can simulate such effects as hydrogen diffusion, hydrogen-hydrogen interaction in non-stoichiometric hydrides, and hydrogen atoms and molecules on metal surfaces. Because of the possibly large amount of computer resources necessary for such an effort, we also have approximate Hartree-Fock cluster programs that employ the iterative extended Hückel method. Because of the capability to "calibrate" the approximate Hückel method against the accurate Hartree-Fock results, it is hoped that much accurate information can be obtained concerning the microscopic behavior of hydrogen in different environments of metal atoms. This information is essential to an understanding of the statistical mechanics of hydrogen in metals. Examples of the type of information that is involved in statistical mechanics treatments of hydrogen in metals are: coordination numbers, vacancy formation energies, and defect-defect interaction energies. It is precisely this type of knowledge, on a microscopic level, that can be obtained from such an approach.
(J. L. Ivey)

PULSE NMR STUDIES

Diffusion Studies in VH_x

Nuclear magnetic resonance (NMR) techniques are being used to investigate the interrelationships between electronic structure, hydrogen atom locations, and hydrogen mobility. Although considerable effort has already been spent in evaluating metal hydride behavior, many questions remain unanswered. For example, numerous studies of hydrogen diffusion have been performed;[6] yet existing theories cannot satisfactorily explain the experimental results for structure changes, phase transformations, or isotope effects. The vanadium hydride system is interesting since three distinct phases (that is, bcc, bct, and fcc) are formed depending upon the hydrogen concentration and temperature. Hence, several factors can be studied in a single hydride system.

The proton spin-lattice relaxation times (T_1) have been previously measured[7] as a function of temperature and resonance frequency for a sample of $VH_{0.53}$. During recent months, these T_1 measurements have been extended to several other VH_x samples over a wider temperature range. In addition, all of the T_1 data has been analyzed to determine the correlation times (τ_c) for proton self-diffusion constants. Vanadium hydride samples with H/V ratios between 0.39 and 1.83 were prepared by reacting hydrogen gas with zone-refined vanadium metal. Subsequent room temperature x-ray diffraction analyses of these materials verified the expected hydride phase for each composition. The T_1 values were measured using a three-pulse technique at a resonance frequency of 23.3 MHz. The proton T_1 values for VH_x are expected to have two major contributions:

$$1/T_1 = 1/T_{1d} + 1/T_{1e}, \qquad (1)$$

where T_{1d} is related to hydrogen diffusion and T_{1e} arises from the contact interactions between protons and conduction electrons. A general expression for relating T_{1d} to the diffusion correlation time τ_c was given previously[7] for metal hydrides. T_{1e} should obey the Korringa relation:

$$T_{1e}\,T = K, \qquad (2)$$

where T is the absolute temperature and K is a constant proportional to the electron density of states at the Fermi energy.

The proton T_1 data for four VH_x samples are shown in Figure 6. The minima indicate the major relaxation mechanism is hydrogen self-diffusion. Breaks in the T_1 temperatures dependences are observed at ~450 K and coincide with the phase transition[8] from the bct β-phase (low temperature) to the bcc α-phase (high temperature). Since the hydrogen diffusion constants in α-VH_x are[6] $\lesssim 10^{-5}$ cm^2/sec, diffusion cannot significantly influence the nuclear relaxation rates and T_1 is caused by the hyperfine interactions with conduction electrons. The concentration dependence of the Korringa constant (K_α) for α-VH_x is given in the second column of Table 4. The increase K_α with hydrogen content agrees with the recent measurements of Kazama and Fukai[9], who interpreted the increase in terms of positively ionized protons donating their electrons to rigid vanadium electron bonds. However, this behavior for K_α is also consistent with more rigorous band theory calculations[10] where the hydrogen electrons go into primarily metal-like states and tend to fill the metal conduction band. Since the emphasis of the present study is to evaluate the diffusion characteristics, the T_1 results for α-VH_x will not be discussed further.

Diffusion is believed to be the major contribution to T_1 for β-phase VH_x above ~200 K. Hence, analysis of the T_1 data should provide information on β-VH_x diffusion parameters. Previous work[7], indicated the vanadium-proton dipolar interactions should dominate T_{1d}; and τ_c can be evaluated using the BPP model[11] expression:

$$1/T_{1d} = \frac{2}{5}\frac{C_S}{\omega_I}\frac{110.2}{a_o^6}\left[\frac{y_I/3}{1+(y_I-y_S)^2}+\frac{y_I}{1+y_I^2}+\frac{2y_I}{1+(y_I+y_S)^2}\right], \qquad (3)$$

where C_S is a constant, ω_I is the proton resonance frequency in radians-1, ω_S is the vanadium resonance frequency, a_o is the lattice constant, $y_I = 1/\omega_I\,\tau_c$, and $y_S = 1/\omega_S\tau_c$. In practice Eq. (3) is not used to determine τ_c. Instead, the ratio of T_{1d} to the experimental minimum for T_{1d} (that is, T_{1min}) is used to obtain the expression:

$$T_{1d} = 1.4913\,T_{1min}\left[\frac{y_I/3}{1+(y_I-y_S)^2}+\frac{y_I}{1+y_I^2}+\frac{2y_I}{1+(y_I+y_S)^2}\right]^{-1} \qquad (4)$$

A computer program has been written to calculate τ_c from Eq. (4). Although this program currently applies only to the vanadium-proton interactions, it can be readily modified to determine τ_c for either proton-proton or other metal-proton interactions.

The τ_c values for β-VH_x have been determined from the experimental T_1 values after assuming the T_{1e} contributions are negligibl

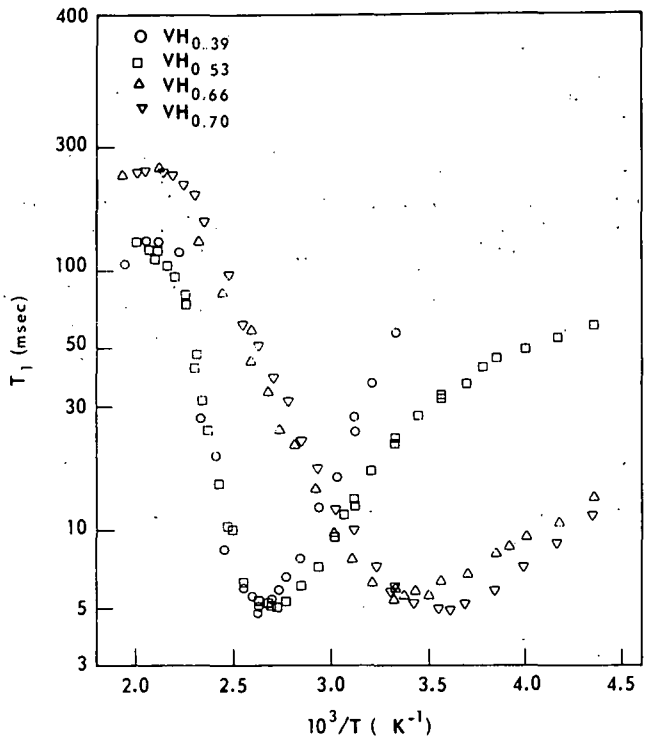

FIGURE 6 - Temperature dependence of the spin-lattice relaxation times T_1 for proton in samples of vanadium hydride. The resonance frequency is 23.30 MHz.

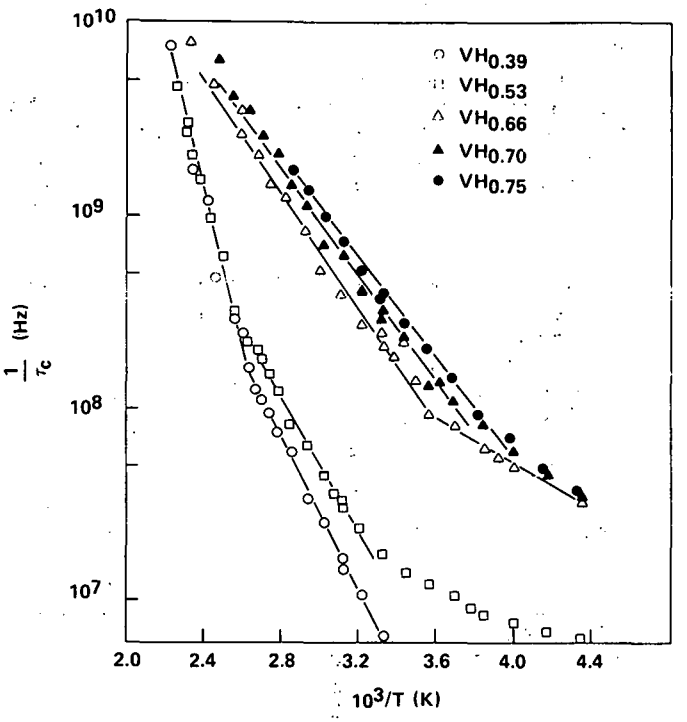

FIGURE 7 - Temperature dependence of jump frequency (τ_c^{-1}) for proton diffusion in β-phase VH_x having various hydrogen concentrations.

Table 4

SUMMARY OF NMR DATA FOR PROTONS IN VH_x SAMPLES -ν = 23.3 MHz

Sample	K_α (s K)	T_{min} (K)	E_a (eV)	τ_∞^{-1} (Hz)	D (300 K) (cm^2/sec)
$VH_{0.39}$	59	380	0.38$_5$	3.2×10^{12}	8.2×10^{-10}
$VH_{0.53}$	56	367	0.30	3.5×10^{11}	2.2×10^{-9}
$VH_{0.66}$	119	291	0.29	2.7×10^{12}	2.7×10^{-8}
$VH_{0.70}$	114	282	0.29	4.5×10^{12}	3.9×10^{-8}
$VH_{0.75}$	---	276	0.27	1.9×10^{12}	4.6×10^{-8}

(which should be valid near the T_1 minima). The temperature dependence of τ_C^{-1} is shown in Figure 7 for five VH_x compositions. Near T_1 minima, the τ_C appear to obey the Arrhenius relation:

$$\tau_C = \tau_\infty \exp(E_a/kT), \quad (5)$$

where E_a is the proton diffusion activation energy, τ_∞ is the frequency factor, and k is the Boltzmann constant. Their parameters are given in Table 4 along with the calculated diffusion constant (D) at 300 K obtained using:

$$D(300) = \frac{1}{6} \frac{\langle\lambda^2\rangle}{\tau_C(300)} . \quad (6)$$

Here, $\tau_C(300)$ is the diffusion correlation time at 300 K and the mean squared hydrogen jump distance $\langle\lambda^2\rangle$ is assumed equal to the shortest distance between the octahedral sites along the c-axis of the bct vanadium lattice. However, the τ_C data for each VH_x composition do not follow a single Arrhenius equation throughout the measured temperature ranges. Although this behavior may be partially due to inadequacies of the BPP model, particularly at lower temperatures,[11-13] the complexities of the VH_x phases are also responsible. The sharp breaks in τ_C for $VH_{0.39}$ and $VH_{0.53}$ above ~385 K may indicate the presence[14] of a new phase between α and β-phases. Also, below ~200 K, the β-phase hydrogen atoms reorder[15,16] to form additional phases with complex superstructures. Since the sites occupied by the hydrogen atoms probably change during these phase transformations, significant variations in proton mobilities are expected. Unfortunately, the current T_1 data is not sufficient to evaluate these complex effects. Nevertheless, the parameters in Table 4 are believed to be representative of the diffusion behavior in β-VH_x at temperatures near the T_1 minima. Here, increases of the hydrogen content in β-VH_x decrease E_a while increasing D (300 K) by a factor of ~50. Increases in the hydrogen content in a fcc metal hydride such as TiH_x[12,17] produce no change in E_a and a decrease in the hydrogen diffusion rate. Since a vacancy mechanism[12] adequately represents proton diffusion in the fcc case, the significant differences for β-VH_x suggest another type of process may be responsible. However, due to the complexities of the VH_x phase relations, additional study is required. Consequently, the T_1 measurements are being extended to lower temperatures as well as the use of other NMR techniques (that is, determinations of T_2 and $T_1\rho$) to evaluate the influence of phase changes on hydrogen diffusion.

Studies of $FeTiH_x$

Previous NMR measurements[7] of the two $FeTiH_x$ phases indicated that the proton resonance signals were inhomogeneously broadened. Since impurities could be responsible, additional $FeTiH_x$ samples were synthesized using FeTi obtained from Alfa-Ventron rather than material prepared at Mound. Preliminary NMR measurements of these new $FeTiH_x$ samples, indicate little difference for either the proton line shapes or relaxation times from the original material. Hence, the inhomogeneous fields are probably caused by the intrinsic paramagnetism of $FeTiH_x$. NMR investigations of $FeTiH_x$ are being hampered by the severe restrictions placed on the equipment by the very rapid signal delay times. However, improved techniques and modified equipment are currently being used to evaluate both proton structures and diffusion in the $FeTiH_x$ phases.

(R. C. Bowman, Jr., A. Attalla, and W. E. Tadlock)

EXISTENCE OF PENTAVALENT PLUTONIUM IN THE ENVIRONMENT

Recently, an interesting paper describing many experiments on the behavior of plutonium in various soils has appeared.[18] This paper concludes that a likely form of plutonium in environmental circumstances is tetravalent plutonium, a conclusion which appears at present to be very reasonable. This paper also concludes that the existence of pentavalent plutonium in the environment is most unlikely because the formal reduction potential of the

$$PuO_2^+ - Pu(OH)_4$$

couple has the high value of about +1.1 V. It may be that pentavalent plutonium is an unimportant and negligible form of plutonium in the environment, as the authors of this paper suggest; but the absence of pentavalent plutonium in the environment is likely to derive from reasons more diverse and profound than impressions that may be derived from examinations of one value of one formal potential. Although Pu(V) may be absent from environmental systems, mere examination of the $PuO_2^+ - Pu(OH)_4$ formal potential is insufficient to establish this conclusion beyond all further doubt.

The formal reduction potential of the $PuO_2^+ - Pu(OH)_4$ couple refers to the imagined equilibrium between solid hydrous plutonium (IV) oxide and pentavalent plutonium ions, the latter at unit (one molar) concentration. This is an equilibrium that is most unlikely to ever be encountered under environmental circumstances. The actual potential of the $PuO_2^+ - Pu(OH)_4$ equilibrium in other circumstances depends upon the particulars of the other circumstances. Many of these particulars cannot be dismissed as unimportant. For example, the actual potential of the $PuO_2^+ - Pu(OH)_4$ couple depends upon the concentration of the pentavalent plutonium. If the pentavalent plutonium were 10^{-13} M, a value which may possibly be found in some environmental circumstances, the $PuO_2^+ - Pu(OH)_4$ potential no longer has its high value of +1.1 V; but instead, this potential is reduced to about +0.3 V, a value which is not so large as to appear overwhelming. Hence, a change in the concentration of Pu(V) to a value that is reasonable for environmental conditions changes the psychological aspect of the problem considerably, since there is no longer the necessity to face a rather impressive value for the potential of the plutonium redox couple of interest. The formal potential value of the Pu(V) - plutonium (IV) hydroxide couple, or the real potential of this couple under diverse circumstances, also depends upon the value of the solubility product of the plutonium (IV) hydroxide. A commonly used value for this solubility product is about 10^{-55}. But this number cannot be assumed to be invariably accurate, for there is considerable doubt about the numerical value of this solubility product, as Perex-Bustamante has pointed out.[19] (Indeed, there is even doubt about the applicability of the solubility product principle to very low quantities of very insoluble materials-see the Appendix in Reference 20). Moreover, the solubility product of very fine particles of hydrous plutonium (IV) oxide such as may occur in the environment cannot be assumed to be identical to the solubility product of macroscopic amounts of this hydrous oxide, because there are considerable surface free energy effects associated with finely dispersed particles. (A pleasingly readable exposition of this point of view can be found in the little book by Alexander[21].) Fine particles of plutonium (IV) hydroxide, such as can occur in the environment, may result in an increased solubility of the hydroxide; an effect which would further lower the real value of the potential of the $PuO_2^+ - Pu(OH)_4$ couple.

Implicit in discussions of plutonium in the environment is the assumption that plutonium (IV) hydroxide is one of the most "stable" forms of plutonium, and that this hydrous oxide, by virtue of its low solubility, limits the concentration of all other plutonium ions. But the idea that $Pu(OH)_4$ is the most important, or one of the most important, species at very low plutonium concentrations is an idea which, while convenient, could bear confirmation. There is yet another factor that can affect the real potential of the $PuO_2^+ - Pu(OH)_4$ system in the environment. Nature can produce a variety of complexons; some of these complexons are suitable for complexing the unipositive alkali cations. (Even the common complexon EDTA shows sequestering ability for the sodium ion). It cannot be assumed that

nature is incapable of providing powerful complexing agents for the ion of Pu(V). Such complexing of the ion of pentavalent plutonium will have the affect of further reducing the real potential of the Pu(V) $Pu(OH)_4$ couple.

When considering the unimportance of an oxidation state of such plutonium as may be dispersed in the environment, it is desirable to define what is meant by the word "unimportant." In connection with pentavalent plutonium, this word may mean unimportant in comparison with the total plutonium at hand, or it may mean unimportant with regard to the soluble plutonium that is present. "Unimportant" in the first case does not necessarily imply "unimportant" in the second case. Several years ago, a discourse on the characterization of plutonium in natural waters was presented.[22] This paper considered only the distribution of soluble valence states and showed how "important" or "unimportant" might be quantitatively assayed. This assay depended upon a simple calculation involving the pH of the environmental system, the redox potential of the environmental system, and the ability of the environmental system to sequester the various plutonium ions. In the climate of environmental concern that prevails today, it would appear desirable to assay plutonium valence state distributions explicitly, rather than to depend upon such impressions as may be conveyed by formal or standard potentials. (To confuse real and formal potentials is to confuse ΔG and $\Delta G°$. By this reasoning, Pu(V) should be the most abundant ion of plutonium, since its standard free energy of formation is more negative than that of any other plutonium ion. In most cases, it is found that Pu(V) is one of the least abundant plutonium ions.)

It may be of interest to remark that, however much formal and standard potentials of plutonium may be used to control the behavior of plutonium and other chemicals in the laboratory, such formal potentials are unlikely to obtain the upper hand in natural circumstances. Where plutonium occurs in nature as a miniscule component, it is not the potentials of plutonium couples that are likely to dictate the natural circumstances but rather the environmental circumstances that are likely to dictate the potential; and the plutonium may be obliged to adjust accordingly. The inherent potentials of many natural systems derive from the biological processes occuring in those systems and are likely to be of great importance is assaying the distribution of plutonium valence states.

The calculation of plutonium valence state distributions is conceptually very easy, and it is curious that this approach has never obtained much consideration. Of course, this approach is not without difficulties of its own. Paramount among these difficulties is the fact that such calculations, however carefully and thoughtfully executed, refer to equilibrium circumstances only; and there is no information on the time required for plutonium to reach equilibrium in environmental circumstances. Establishment of equilibrium may require years, so that studies of plutonium in natural systems may be limited to empirical observations. While the rates of oxidation-reduction reactions often decrease rapidly with decreasing concentration of the reactants, it nevertheless might be interesting to try to estimate the equilibrium distribution of plutonium valence states without prejudicial rejection of one or more of these oxidation states. Whether this can be done by a technique such as solvent extraction, which may upset and disturb the natural order of valence state arrangements (and therefore yield misleading results), is an interesting and unresolved question. *(G. L. Silver)*

PROBLEMS IN PLUTONIUM CHEMISTRY (II): PLUTONIUM AS A CONCENTRATION "CARNOT" FLUID

Currently, there is much interest in the use of plutonium as a fuel for electric power generation by nuclear fission. But it is also possible to use plutonium to generate small amounts of energy by taking a dissolved sample of plutonium around an "aqueous Carnot cycle". The oxidation-reduction potentials of plutonium are acid dependent: more energy can be obtained by reducing a sample of plutonium at high acidity than is expended by reoxidizing the same sample at a low acidity. The following example, which is shown in Figure 8, serves to illustrate how this may be used to obtain electrical energy. Small acidity changes caused by disproportionation reactions and oxidation or reduction of the plutonium have been neglected, as had hydrolysis.

An exhibition of commercial nuclear machinery is held in a hot, arid, country. To stimulate interest in nuclear technology, it is decided to run a sample of plutonium around "Carnot"-type cycle to extract a small amount of electrical energy to lift a tiny weight, such as a feather. A one liter sample of 0.03M plutonium in 3M acid is placed in a display case and connected to a normal hydrogen electrode.

The average oxidation number of the plutonium (N) is initially 5.8. By means of circuitry, which contains a tiny capacitor and coulometer, the cell is now discharged until N = 3.2. The cell is disconnected and two liters of water are very carefully added to dilute the acid concentration in the plutonium cell from 3M to 1M. Stored energy from the capacitor is then used to reoxidize the plutonium to N = 5.8. Water from the cell is allowed to evaporate into dry air until the acid concentration is again 3M. The cell has now been returned to its initial condition. This initial condition is denoted by point "A" in Figure 8, which plots the log of plutonium solution acidity against the log of the ratio of hexavalent to pentavalent plutonium, denoted M. Discharging the plutonium battery from N = 5.8 to N = 3.2 at constant acidity is represented in Figure 8 by the vertical line connecting points A and B. The work available along the line from A and B is approximately -1.916 kcal. At constant average oxidation number (3.2), the plutonium solution in now diluted with water (line BC from point "B" to point "C"). This process is done manually by an attendant who would have been paid anyway, so that work from B to C may be neglected. From C to D, the plutonium is reoxidized from N = 3.2 to N = 5.8 by means of the energy stored in the capacitor. The work associated with this charging process is approximately 1.846 kcal. Evaporation of water is spontaneous in the desert air, so that work in this step may be neglected. This step ("D" to "A") returns the plutonium solution to its initial condition. But recharging the battery for the next cycle did not require quite as much energy as was obtained from discharging the battery. The difference, about 70 cal, could be used to lift a tiny weight a short distance. *(G. L. Silver)*

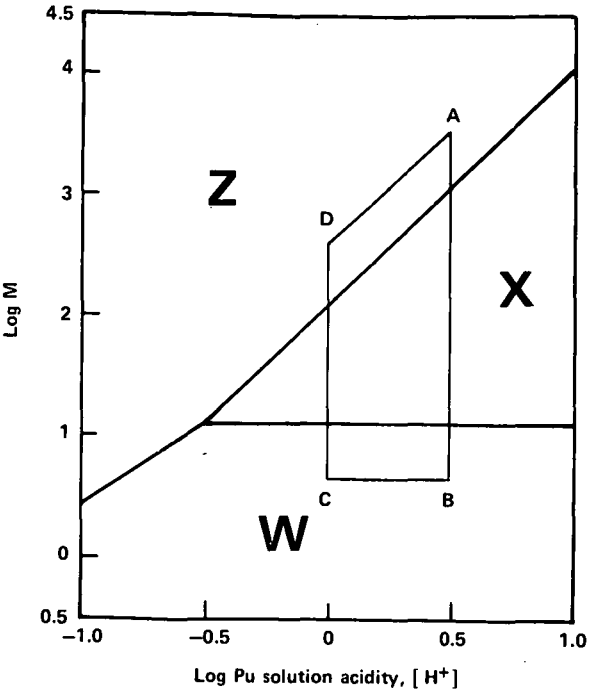

FIGURE 8 - A concentration "Carnot" cycle for plutonium imposed upon a partial plutonium predominance region diagram [W = Pu(III), X = Pu(IV), Z = Pu(VI)].

PROTACTINIUM-231 AND THORIUM-230

Mound Laboratory recovers thorium-230 and protactinium-231 from a uranium mill by-product known as Cotter Concentrate and ships the products to the Heavy Elements Isotope Pool at ORNL. Previous reports[23-25] have described in detail the origin and character of the Cotter Concentrate, the facilities, and the development of the current recovery and purification process. Briefly, the process consists of leaching about 20 liters of solids in hot, concentrated nitric acid and diluting and filtering off the insoluble residue. Uranium is extracted from 90-liter batches of filtrate by multiple contracts with 8-liter portions of 10% DSBPP/CCl_4 (di-sec-butyl phenyl phosphonate in carbon tetrachloride) and stripped from the organic with 0.005M nitric acid. Thorium is extracted from the filtrate by multiple contacts with 0.1M TOPO/CCl_4 (trioctyl phosphine oxide in carbon tetrachloride), with each contact followed by a 0.3M sulfuric acid strip. After the thorium has been removed from the filtrate, further contacts with TOPO/CCl_4, each followed by an 0.5M oxalic acid strip, result in recovery of the protactinium. Uranium strip solutions are precipitated with ammonia and the precipitate collected for eventual return to the uranium processor. The thorium strip solutions are purified by an oxalate precipitation and then calcined to the oxide. Protactinium strip solutions are concentrated by evaporation after which they are purified by a series of precipitation steps. The process is summarized in a process flow diagram that is shown in Figure 9.

Since the last semiannual report,[25] 11 additional batches of Cotter Concentrate have been processed from drums (No. 178 and 177).

A shipment of 40.58 g of purified thorium-230 was made on June 20, 1975 to the Heavy Elements Isotope Pool at ORNL. Thorium-230 currently on hand from FY-1976 production totals 44 g. Unpurified protactinium-231 recovered from the 11 batches is estimated, by gamma spectra analyses, to be approximately 100 mg.

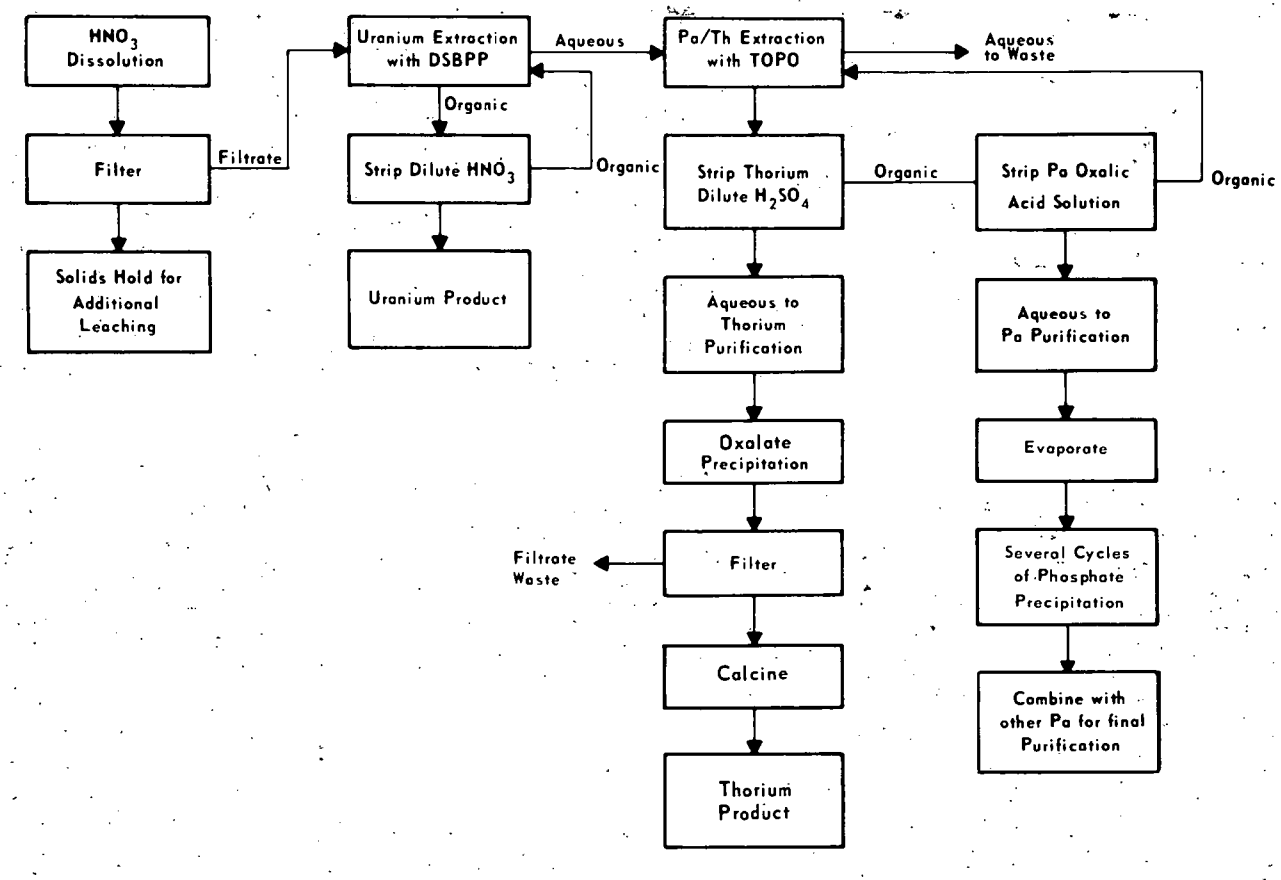

FIGURE 9 - Pa/Th recovery and purification from Cotter Concentrate.

The thorium-230 value was based on calorimetry using a half-life of 80,000 yr. The calculated ^{230}Th/total oxide ratio was 0.02725. Emission spectrographic analysis showed Sc to be the major impurity (1%) with small amounts (0.1% or less) of Zr, Si, P, Na, B, Y, Ca, Mo, Fe, Al and Cu. Assuming total impurities of 2%, the isotopic composition (% ^{230}Th in total Th) was calculated to be 3.16%.

As reported earlier,[25] a considerable portion (40%) of the Pa in the original Cotter Concentrate does not dissolve in the nitric acid leach and remains with the insoluble residues. Various methods of recovering the Pa are being tested. When 750 g of residue was treated with a total of 11.5 liters of 3M NaOH at 100°C, the volume of solids was reduced greatly; and some organic material was removed. The caustic leach solution contained negligible amounts of Pa and ^{230}Th. When the solids were then leached and hot 0.5M oxalic acid, nearly all of the Pa, but little of the ^{230}Th, was removed. Additional work on testing and refining this technique is in progress.

Piping, pumps, and electrical connections have been installed on the two Karr, three-inch, reciprocating plate, liquid-liquid, solvent extraction columns and initial test operation is underway. These columns were purchased and set in place in FY 1975.[25] Initial operation is for a test of DSBPP/CCl_4 extraction and stripping of the uranium content of the Cotter Concentrate feed filtrate solution.

In the early development work, little time was spent on the detailed procedures for purifying Pa. Protactinium was recovered from the oxalate strip solutions by a manganese dioxide carrier precipitation, and the precipitates were stored pending further processing. A Pa purification procedure is being developed concurrently with production of Pa.

Two difficulties were encountered with the manganese dioxide precipitation procedure, namely, the excessive amount of attention required during the addition of permanganate and problems with filtering and handling the MnO precipitates. Other methods of concentrating the Pa have now been considered. Since small-scale tests indicated that the oxalate strip solution could be evaporated at least 20-fold without problems, an evaporator was set up. A three-liter, round bottom flask was equipped with a water-cooled condenser and a heating mantle with a temperature controller. A "chicken feeder" type liquid-level control with a 20-liter reservoir was added. This system has been in operation for six months, has worked well, and has required very little attention. Data from evaporation batches are given in Table 5. Volume reductions of up to 40 have been achieved, but a slight problem has developed. Each evaporated batch contains a small amount (2-20 ml volume) of precipitate that is filtered and analyzed by gamma counting. As shown by the data on Batch 7, large volume reductions can result in appreciable amounts of Pa in the solids. However, Pa precipitation can occur even with modest volume reduction as shown for Batch 6. A possible explanation is that varying amounts of impurities accompany the Pa in the oxalate strip solution, as has been observed during processing of different drums of Cotter Concentrate. Acidity determinations on evaporated solutions showed 7-9M acid, indicating appreciable extraction of nitric acid during the solvent extraction step.

An attempt to recover Pa from the evaporated oxalate solution by MnO_2 carrier precipitation was not successful. A solution was diluted to 2.7M HNO_3, a small amount of oxalic acid added, heated to 80°C, and $KMnO_4$ added until MnO_2 formed; but the precipitate carried only 2/3 of the Pa. This may have been caused by the acidity being too high or to the concentration of other impurities that prevented complete precipitation of Pa.

Table 5

SUMMARY OF EVAPORATION BATCHES

Batch	Strip Soln. Vol.	Strip Soln. Pa(mg)	Vol. Red.	Product Soln. Vol.	Product Soln. Pa(mg)	Product Soln. %	Solids Pa(mg)
2	20	13	13	1.5	8.1	62	n.a.
3	20	12	12	1.72	14.5	121	0.7
4	32	20.2	24	1.32	15.3	76	1.6
5	52	26.1	25	2.04	12.8	49	1.3
6	24	13.3	14	1.67	3.2	24	8
7	24	9.3	40	0.60	6.5	70	4.4

Protactinium was recovered from the evaporated oxalate solution by a phosphate precipitation. After diluting the solution to 2-3M HNO_3, phosphoric acid was added to a concentration of 0.075M, and the solution heated. At 70°C, the precipitation began and seemed to be complete after 10-20 min. The precipitate was digested for several hours and cooled overnight before collecting the precipitate on filter paper. The optimum conditions for the precipitation have not yet been established; but after a relatively few precipitations, under varying conditions, the following observations seem germane:

1) The precipitation is relatively slow. When the solution was heated to 70°C or above before the addition of the H_3PO_4, up to five minutes elapsed before the solution became cloudy and precipitation seemed to occur at the same rate as the case for prior addition.
2) The precipitation always seemed to occur at about 70°C if sufficient H_3PO_4 were present.
3) The precipitates were voluminous and gelatinous. The volume of precipitate, calculated from the estimated thickness of the filter cake, was often 100-200 ml. Air-dried filter cakes had a much smaller volume, which was difficult to estimate.
4) The precipitate itself was white but usually carried enough solution to be slightly colored. The supernatant solution was a bright blue-green color, very similar to the color of the starting solution.
5) Some minimum amount of H_3PO_4 seemed to be required before any precipitation occurred; but if precipitation occurred, all of the precipitate came down (This observation could have been caused by the relatively large increment of H_3Po_4 addition. Addition of "excess" H_3Po_4 seemed to have no effect.
6) Under the "proper" conditions, the filtrate solutions contained negligible amounts (less than 0.1 mg) and were discarded.

Initial attempts to dissolve the phosphate precipitation cake in warm 0.5M oxalic acid left a residue containing minor, but recoverable, amounts of Pa. However, leaching the filter cake with hot 1M NaOH converted the precipitate to a form that was easily and completely soluble (probably because of removal of the phosphate). When HCl and H_3PO_4 were added to concentrations of 1M and 0.075 M, respectively, and the solution was heated to 70°C, the resulting precipitate seemed the same as the previously described precipitate. These second cycle precipitates were pure white, gelatinous, and only slightly less voluminous than those from the first cycle. Most of the comments and observations recorded for the first cycle precipitation also apply to the second cycle precipitation, with the added complication that the concentration of HCl becomes another variable factor. Dozens of the precipitations from the oxalic/HCl medium have been run with the majority giving 99% recovery of the Pa and discardable filtrate solutions. In the few cases where Pa loss was excessive, additional HCl, or H_3PO_4, or both (and heat) produced acceptable recovery of the Pa. After leaching with hot 1M NaOH, the precipitates were easily soluble in warm oxalic acid; and the precipitation could be repeated.

The success of this technique suggested the possibility of direct precipitation of the Pa from the nonevaporated oxalate strip solution. An oxalate strip solution containing 2.9 mg Pa was adjusted to 1.1M HCl and 0.07M H_3PO_4 and heated to 75°C. The resulting precipitate was digested 2 hr and cooled overnight. The filtrate solution containing 2% of the starting Pa and was discarded. Thus, the direct precipitation on the oxalate strip solutions could be considered an alternate procedure for the manganese dioxide precipitation.

Manganese dioxide carrier precipitates were processed by dissolving the solids in hot (80°C) oxalic acid, adding HCl and H_3PO_4 and precipitating by the standard procedure. Materials processed in this way appeared and behaved identical to the material derived from evaporated strip solutions. The initial oxalate solution was the typical blue-green color, and this color disappeared completely in two precipitation cycles. The appearance, behavior, and amount of precipitate seemed no different from previous precipitates; and after two cycles of precipitation, Pa from both sources was combined.

Continuation beyond two cycles of precipitation resulted in little "apparent" reduction in the volume of precipitates. During previous work on dissolving low level residues, it had been observed that H_2O_2 aided dissolution and produced either yellow or bright red solutions. The addition of H_2O_2 to the precipitation medium (1M HCl, 0.5M oxalic acid, 0.75M H_3PO_4) resulted in additional separation of impurities, and a much more complicated system. Some of the peroxide complexes (namely, colored solutions) were stable at temperatures of 90°C and above and seemed to prevent precipitation of the impurity while permitting the Pa to precipitate. In contrast to previous experience, the resulting precipitate seemed to be affected

somewhat by the amount of H_3PO_4 present and the temperature (above 70°C). The precipitate was crystalline rather than gelatinous, small in volume, and settled to the bottom of the beaker within a few minutes. The protactinium content of the filtrate was variable, often high, and in at least one case, increased upon standing.

By use of the above described methods, two batches of Pa totaling 100 mg were concentrated until the centrifuged volume of hydroxide precipitate was less than 20 ml. These batches have been dissolved in sulfuric acid in preparation for the next purification step. *(P. E. Figgins, M. R. Hertz, and W. S. Stringham)*

STUDY OF THE REACTION OF PLUTONIUM WITH BONE CHAR

Bone char is being studied as an adsorbent for removing traces of plutonium from waste water that is to be discharged to the environment. Previous work on the properties of bone char have included a literature search of bone char properties, an analysis of a typical sample of the bone char, and a description of the behavior of the bone char-water system.[26,27]

New samples of bone char have been prepared, sized to 74-105μ with standard sieves, and washed several times with water to remove fines. To ascertain whether this new sample of bone char had properties which approximated the previous samples, the potential-pH behavior of the bone char was examined. Figure 10 shows this potential-pH behavior in a carbonate buffer, whereas Figure 11 shows this behavior in a phosphate buffer.

The potential increased with decreasing pH in the expected manner, which indicated that this potential-pH behavior seems to be intrinsic to the bone char system and is not affected by screening and washing the bone char (whether this potential-pH behavior is the same for bone char obtained from other commercial suppliers is not known, however). The samples indicated the same low poising capacity as previous samples, that is, all of the potentials drift upwards upon exposure of the bone char-water systems to air, so that the observed potential depends upon the time of the potential reading. As indicated by Figures 10 and 11, however, if the procedure for taking potential measurements is standardized, linear plots can often be obtained. Because of the potential instability and apparent dependence upon exposure to atmospheric oxygen, it seems likely that the potential is not a useful parameter for describing the bone char-water-plutonium reaction; and for this reason, potential measurements upon such systems have no longer been obtained.

One of the problems accompanying the study of the behavior of plutonium with bone char is that of ascertaining the oxidation state and form of the plutonium in equilibrium with the bone char. Problems associated with the preparation of hexavalent plutonium have already been described.[27]

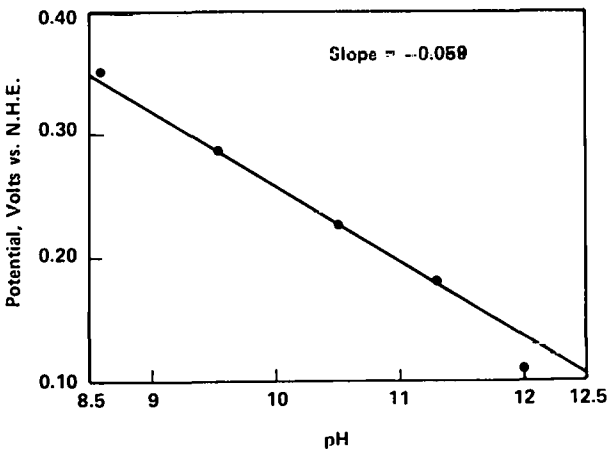

FIGURE 10 - Potential-pH behavior of bone char containing trace Pu (carbonate buffer).

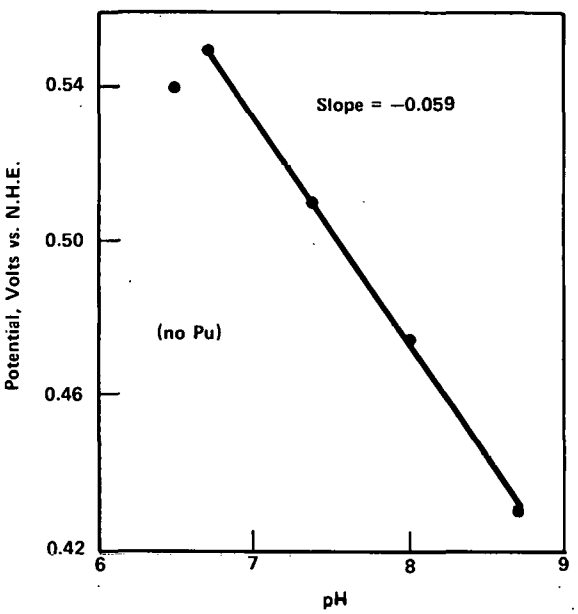

FIGURE 11 - Potential-pH behavior of bone char (phosphate buffer).

After the preliminary examination of the problems associated with the preparation and use of hexavalent plutonium, it was decided to attempt to prepare samples of tetravalent plutonium polymer for equilibration with bone char. The preparation was attempted in the following manner. About 50-100 mg of sodium nitrite were added to about five ml of plutonium-238 stock solution (oxidation state unknown) in 6M nitric acid. This solution was then diluted with 20-25 ml of concentrated (16M) nitric acid. The solution that resulted was then stirred and heated on a hot plate until evaporation had reduced the volume of the solution to about 2 ml. This solution was then cooled and treated with the various test procedures shown in Table 6. Table 6 describes various test procedures for preparing tetravalent plutonium polymer, but it is important to observe that the results quoted in the table are not reproducible. However, since boiling the plutonium solution at pH 12.5 seemed to give the greatest radioactivity decrease upon centrifugation in these preliminary studies, it was decided to use this technique to examine plutonium solutions in the presence of bone char, assuming that the technique did yield solutions of plutonium (IV) polymer. Plutonium solutions prepared by boiling in potassium hydroxide were used to try to ascertain the optimum pH range for removing plutonium from waste water with bone char. The results on one typical study are shown in Figure 12, which plots plutonium-238 counts per minute per 500λ of 100 ml solutions each containing 1 g of bone char. The various pH values were obtained with ammonia buffer. Although the data are scattered, the fact that the activity in equilibrium with the bone char decreases with decreasing pH is evident. Prior to counting, each sample plotted in

Table 6

TEST PROCEDURES FOR PREPARING PLUTONIUM (IV) POLYMER

Procedure Discription	Percent solution radioactivity decrease by centrifugation at 10,000 rpm for 10 min
Pour Pu solution into NH_3 buffer at pH maintained near 10	~ 2
Pour Pu solution into hot NH_3 buffer at pH maintained near 10	~69
Pour Pu solution into boiling water and boil for 5 min	~ 0
Pour Pu solution into a hot solution of 20 ml of concentrated NH_3 + 80 ml water, and then boil for one min.	~79
Pour Pu solution into KOH solution such that final pH was 12.5	~56
Pour Pu solution into 100 ml of boiling water containing KOH such that final pH was 12.5	~90

Figure 12 was centrifuged for 10 min at 10,000 rpm. Figure 13 shows the results of a similar study in carbonate buffer. Figures 14 and 15 show other studies of the bone char-water-plutonium system in a ammonia buffer, but samples were not centrifuged prior to counting. Since there was no centrifugation step to remove large polymer particles, the absolute radioactivity level is increased; but the data again indicate that bone char as an absorbant for plutonium is more effective close to the neutral point than at high pH values. Part of the scatter in the data points in Figures 12, 13, 14 and 15 results from plotting together data obtained from different polymer preparations. As has been previously discussed in works on the chemistry of plutonium, different preparations may lead to different degrees of polymerization; and this is probably as true of preparations that differ only in detail as it is of preparations that differ in other than detail.

In order to examine the behavior of plutonium (IV) "polymer" (prepared by boiling in KOH as described above) in the presence of bone char near the neutral point, two plutonium solutions were prepared for equilibrium in 100 ml flasks with one gram of bone char. Ethylene-diamine was used as the buffer. Plutonium solution No. 1 contained 3571 dis/min/500λ before reaction with bonechar; and plutonium solution No. 2 contained 10,162 dis/min/500λ before reaction with bone char. The results of equilibrating these plutonium solutions with bone char are shown in Figure 16. As can be seen, considerable scatter is inherent in the data. On the average, however, the more dilute plutonium solution gave the lower equilibrium count (about 15 dis/min/ml); and the plutonium solution with the higher initial count gave a higher equilibrium count with bone char (average count about 23 dis/min/ml). It is difficult to obtain data at pH values much below pH 7 because of the tendency of the bone char to dissolve and provide its own phosphate buffer. This self-buffering capacity of bone char tries to adjust the pH to about 8.

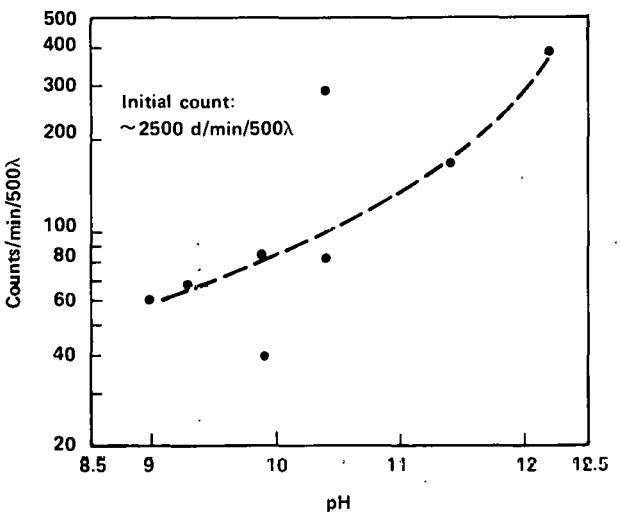

FIGURE 12 - Apparent bone char plutonium (IV) "polymer" equilibrium in ammonia buffer (all samples centrifuged).

During the course of this study, it was observed that the apparent count rate of radioactive samples (stored in polyethylene vials containing the scintillating material and gelling agent) may gradually increase their count rate. This effect first became apparent with samples stored for more than 12 hr. However, this effect did not seem to occur in all samples or to occur uniformly in those samples in which the phenomenon was observed. It has been suggested that this phenomenon may be caused by the slow loss of toluene, a component of the scintillating fluid, through the walls of the polyethylene vials when these vials are stored for long periods at room temperature. A study of this effect was not undertaken since it can apparently be avoided by using glass vials instead of polyethylene vials. In the few cases where the effect was observed, the count rate seemed to increase by about 10-20% in a 24 hr period. This effect may also be from temperature variations in the room, as the variations may encompass a span of 30°F. Data in Figure 16 were obtained by counting all samples in glass vials.

In order to compare the behavior of plutonium (believed to be polymeric) with bone char to plutonium that had received different treatment, a sample of plutonium was first reacted with silver (II) oxide and then allowed to equilibrate with bone char. The reaction with silver (II) oxide was performed to oxidize the plutonium to the hexavalent state prior to reaction with the bone char. Results are shown in Figure 17 and show that plutonium treated as for oxidation to the hexavalent state seems to behave similarly as plutonium treated as for conversion to the polymer.

It seems the scatter inherent in the data illustrated in the figures presented herein is not unknown in the study of radiocolloids. There is no simple, readily apparent reason why such data should intrinsically contain such tolerances; but irreproducibility

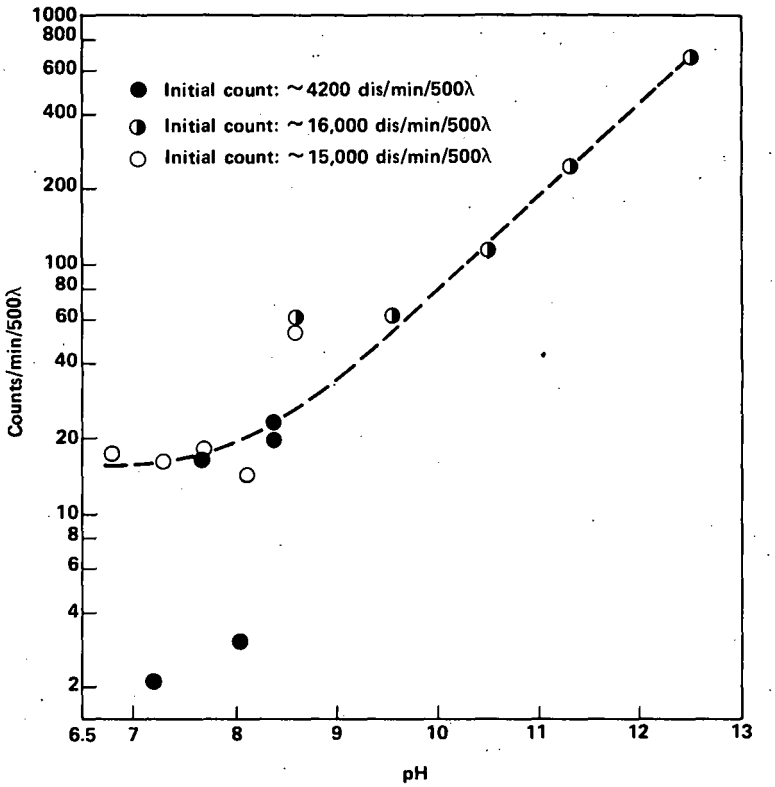

FIGURE 13 - Apparent bone char plutonium (IV) "polymer" equilibrium in carbonate buffer (all samples centrifuged).

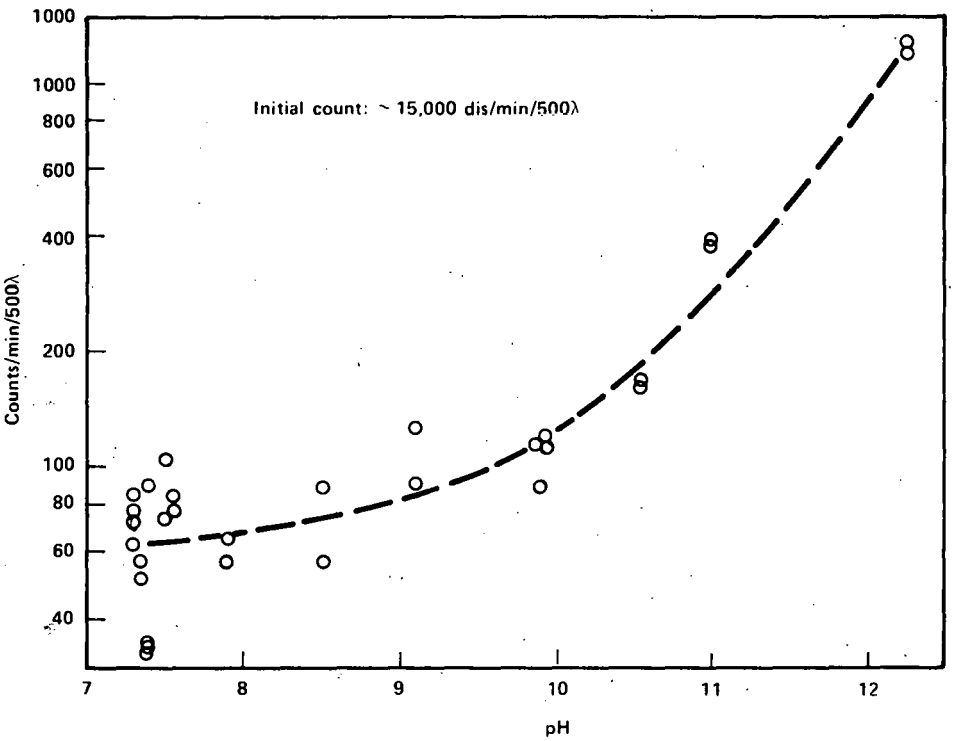

FIGURE 14 - Apparent bone char - plutonium (IV) "polymer" equilibrium in ammonia buffer (samples not centrifuged).

seems to be at least as common in the study of radiocolloids as in other branches of chemistry and perhaps more so. Many workers in the field of radiochemistry have commented upon and attempted to explain the irreproducibility of data sometimes obtained from radiocolloids and sorption systems. There does not seem to be general agreement on what causes irreproducibility of the behavior of radiocolloids, or how to avoid this circumstance. The concentrations of the radiocolloids are often less than the concentrations of impurities in even the highest grade reagent chemicals, and it has been speculated that the behavior of radiocolloids can be attributed to radioelement adsorption upon the impurities present in even the best grades of commercial chemicals, or upon the surfaces of dust particles and the walls of vessels. Egorov has summarized this state of affairs in his statement that: "As a rule, the behavior of radiocolloids on sorption systems is anomalous."[28] In regard to radiocolloid systems and the anomalies often associated with them, Egorov states that: "this problem has in fact no solution."[28] Other workers have also remarked upon the difficulties that seem to be inherent in the study of systems of radiocolloids. Among these commenting workers may be found Mellish, Payne and Worrall[29], Andelman and Rozzell[30], and, in particular, Kepak[31], who has expressed the idea that radiocolloid systems may be examples of systems that are not in thermodynamic equilibrium.

Whatever the nature of radiocolloids or the disagreements and anomalies associated with their study, the adsorption of radiocolloids by glass surfaces can significantly affect the results of sorption studies. It is one of the demonstrations of this section that the effectiveness of bone char as an adsorbent for the removal of one form of plutonium from aqueous solution, the form generated by boiling in aqueous KOH, is greater near pH 7 than at higher pH values (such as pH 11). It is possible, however, that this demonstration is only the result of the absorption of the plutonium by the walls of the glass vessels. A study of the adsorption of plutonium (IV) "polymer" (prepared by boiling in potassium hydroxide) by glass vessels was therefore undertaken. Figure 18 shows the apparent adsorption of the plutonium at several pH values as a function of time that the plutonium solution was allowed to stand in the glass 100 ml vessel. As can be seen from this diagram, the adsorption of plutonium treated as for polymer formation is primarily a high pH phenomenon, and that at pH 10 to about pH 7, the adsorption of the plutonium (IV) polymer by the vessel walls does not seem to be important.

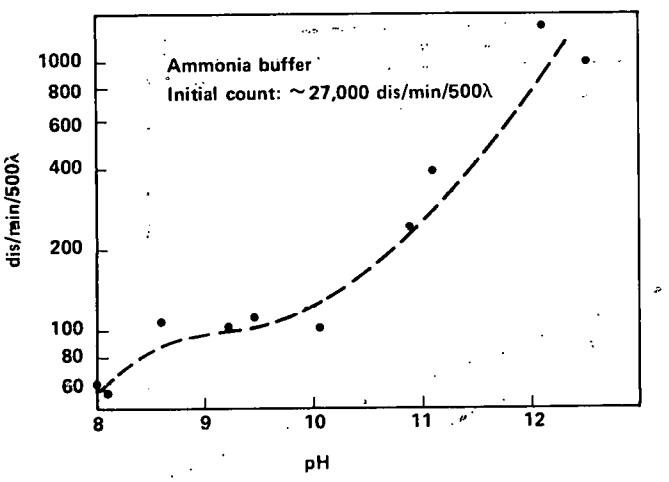

FIGURE 15 - Apparent adsorption of Pu "polymer" by bone char as a function of pH (Dashed line represents one interpretation of data, samples not centrifuged).

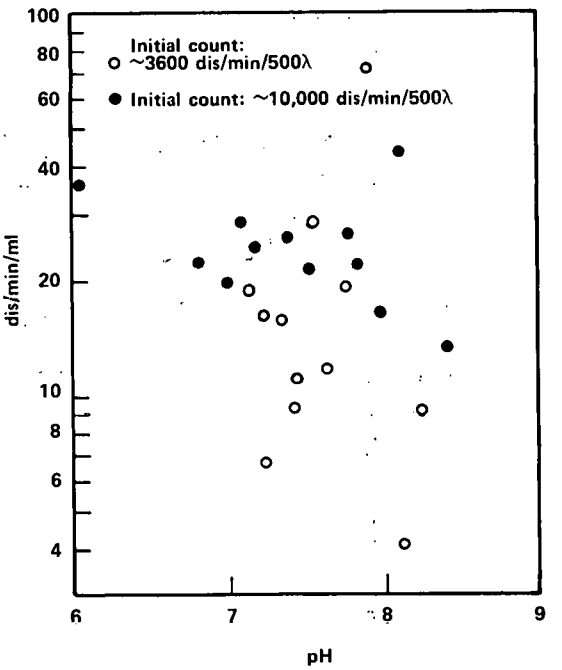

FIGURE 16 - Apparent equilibrium of plutonium (IV) polymer and bone char near the neutral point (Open circles represent solution No. 1, closed circles represent solution No. 2. Ethylene diammine buffer, samples not centrifuged).

The buffer used in this study was ammonia/ammonium nitrate, and each solution was thoroughly shaken prior to sampling. Figure 19 plots the count rate of each solution after 20 days in a glass vessel.

The scatter that appears in the data relating to the adsorption of plutonium by bone char suggests it would be desirable to standardize the plutonium test solutions so that at least the initial form of the plutonium could be stated, and so that the possibility of consistency from experiment-to-experiment can be maximized. As mentioned in the literature of plutonium chemistry, different preparations of plutonium (IV) polymer generally lead to solutions with different adsorption properties. Therefore, a sample of hexavalent plutonium was prepared in nitric acid by oxidation with silver (II) oxide, examined with a spectrophotometer to confirm its oxidation to the hexavalent state, and diluted to an appropriate concentration for use in the study of bone char. Likewise, a stock solution of plutonium (IV) polymer was prepared by precipitation of a sample of hydrous plutonium (IV) oxide

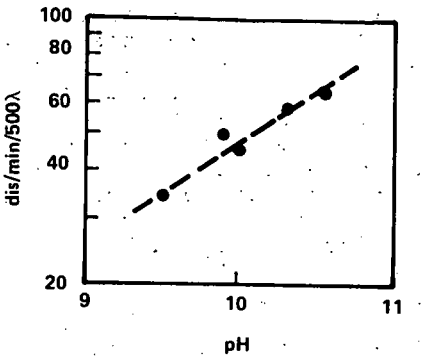

FIGURE 17 - Apparent equilibrium of "hexavalent" plutonium with bone char.

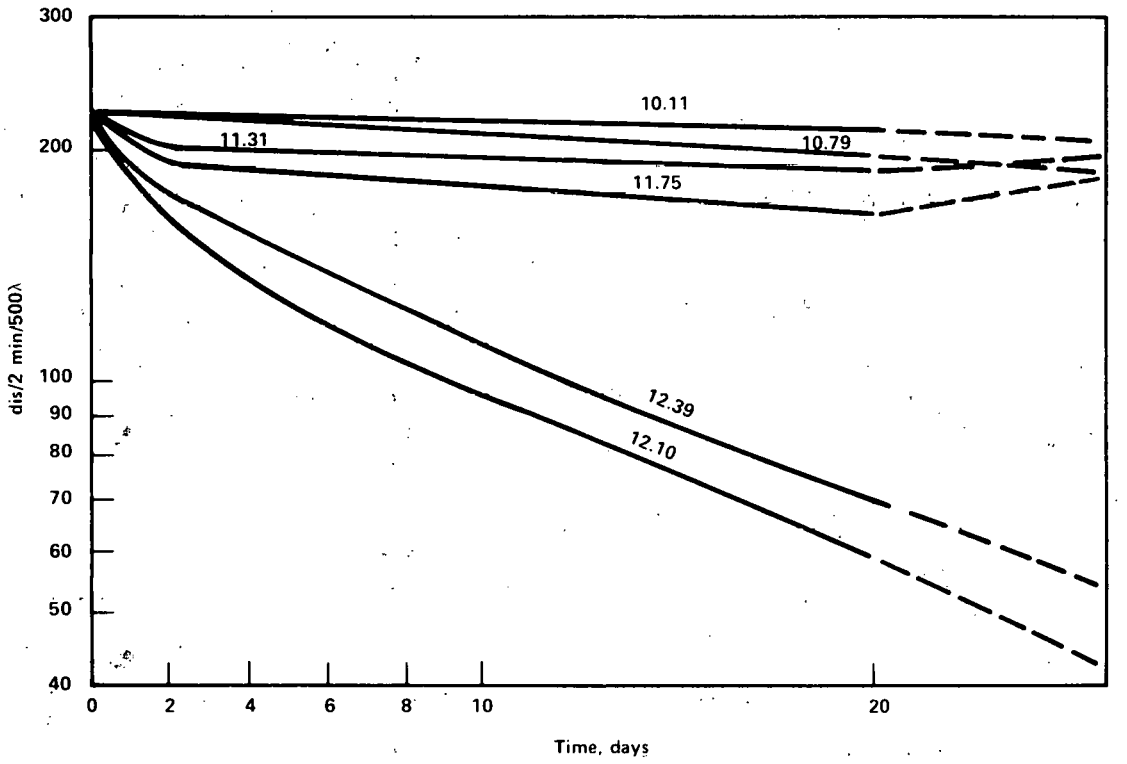

FIGURE 18 - Adsorption of plutonium (IV) "polymer" by glass.

and peptizing this material. Examination of the visible absorption spectrum of this material confirmed that it was polymer, and a sample of this solution was diluted for use in the bone char study. Results of studies on bone char with these standard plutonium solutions will be reported in the future. *(G. L. Silver)*

STUDY OF THE REACTION OF URANIUM WITH BONE CHAR

The objective of this program is to study the mechanism of the removal of uranium in waste streams to ultra low levels. Studies to date have been directed at uranium removal by contacting uranium bearing solutions with bone char, a natural calcium hydroxylapatite. The removal mechanism is thought to be based on the principle of residue adsorption[32]. The hydroxylapatite (HAP) being used in this study is a natural bone char obtained from the Kerr McGee Corporation. Table 7 gives a chemical analysis of this bone char.[33]

Typically, bone char has been used in decolorizing crude sugar syrups and in removing salts or "ash" from process streams. As a result, its physical properties are well known (see Table 8). Other studies of this substance have included the selective adsorption of Sr, Cu, and Mg.[35]

Experimental work in the adsorption of uranium from alkaline and neutral aqueous solutions has continued. The use of adsorption isotherms has been discussed previously[32,36]. Performance of a solid sorption agent in treating a liquid depends upon four factors: stoichiometric capacity of the solid (whenever it can be defined independently), equilibrium behavior (which limits the realization of full stoichiometric capacity), rate behavior (which often further restricts the performance of the system), and process arrangement (with its consequences for the material balance). Sometimes the realizable capacity of a solid has a nearly constant value. In other cases, the effective capacity varies with solute concentration in the feed and thus must itself be determined from the equilibrium behavior.

The behavior of uranium adsorption onto the bone char surface can best be modeled using the Freundlich equation, which relates the amount of uranium in the solution to that adsorbed on the bone char as follows:

$$\frac{x}{m} = k\, C^{1/n},$$

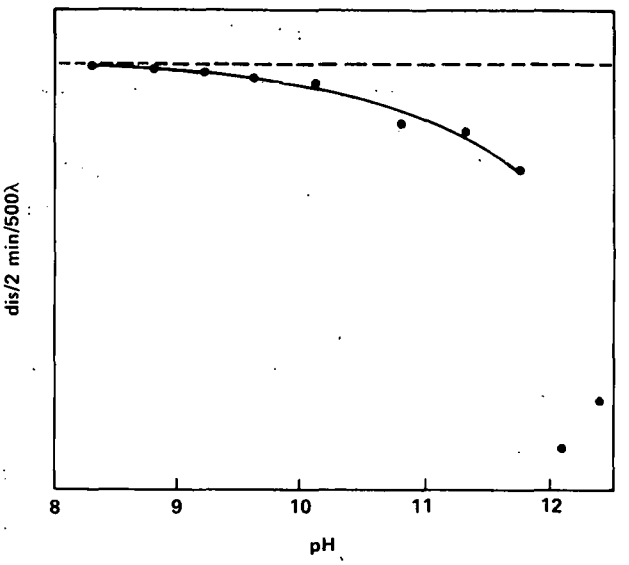

FIGURE 19 - Adsorption of Pu "polymer" by glass count vs. pH after 20 days equilibration (initial solution count given by dashed line).

where:

x = amount of activity adsorbed

m = weight of bone char

k and n are constants

C = unadsorbed concentration of activity left in solution that is in equilibrium with the activity absorbed on the bone char.

The intercept is roughly an indicator of sorption capacity and the slope, $\frac{1}{n}$, of adsorption intensity. The Freundlich equation generally agrees quite well with experimental data over moderate ranges of concentrations, C.

However, the Freundlich equation does not reduce to a linear adsorption expression at very low concentrations such as the Langmuir equation does; nor does it agree well with the Langmuir equation at very high concentrations, since n must reach some limit when the surface is fully covered.

Generally, k and n decrease with increasing waste water complexity. High k and n values indicate high absorption throughout

Table 7

COMPOSITION OF A COMMERCIAL BONE CHAR[33]

Component	Percentage
Ca	33.8
P	15.7
H	0.4
S	0.03
Na	2.4
N	1.0
CO_3^{-2}	5.0
C	5.8
Mg	0.5
Si	0.3
Mn	0.05
Fe	0.1

Table 8

PHYSICAL PROPERTIES OF BONE CHAR[34]

Internal Porosity, %	50-55
External Void Fraction	18
Bulk Dry Density, lb/ft^3	40
Surface Area, m^2/g	100-115
Typical Uses	Decolorizing of crude sugar syrups; removal of salts or "ash" from process streams.

the concentration range studied; conversely, low values indicate low adsorption. A low value of n (steep slope) indicates high adsorption at strong solute concentrations and poor adsorption at dilute concentrations.

Experiments were performed to determine the change in the removal effectiveness of bone char with respect to uranium as a function of pH. Since bone char tends to be slightly soluble at pH's below 7, the pH's chosen were: 10, 8, and 7. The various isotherms generated are shown in Figures 20, 21, and 22. The isotherm at pH 10 was run with ^{234}U isotope; whereas the isotherms at pH 8 and 7 were run using ^{233}U.

In order to compare the various results, the data at pH 10, using ^{234}U, was normalized to ^{233}U data by multiplying the data by the ratios of their respective half lives (Figure 23).

$$\left(\text{dis/min/ml}^{234}\text{U} \times \frac{2.47 \times 10^5 \text{yr}}{1.59 \times 10^5 \text{yr}} = \text{dis/min/ml}^{233}\text{U}\right)$$

The following relationships:

$$\text{pH } 7 \quad \frac{x}{m} = 6 \times 10^{-2} \, C^{2.09}$$

$$\text{pH } 8 \quad \frac{x}{m} = 6.1 \, C^{1.45}$$

$$\text{pH } 10 \quad \frac{x}{m} = 18.6 \, C^{1.21} \quad (\text{normalized to } ^{233}U)$$

were derived by fitting the Freundlich equation to the data, as discussed previously.[32]

One can readily see from Figures 20-23 that pH 10 treatment is better for a batch-type operation since the capacity is greater at equilibrium effluent concentrations. Treatment at pH 7 is better for bone char-column operation since the capacity is greater in equilibrium with a typical influent at column exhaustion. Treatment at pH 8 falls in between the pH 7 and pH 10 treatments. Bone char at pH 10 has a higher adsorption capacity, at low concentrations, than at pH 8 and pH 7. However, at high concentrations the adsorption capacity is highest at pH 7. Also, the adsorption intensity is much higher at pH 7 than at pH 8 and pH 10.

In order to make further comparisons between the pH 7, pH 8, and pH 10 adsorption characteristics of bone char, the various equilibrium distribution coefficients, K_d, were determined; using the three fitted Freundlich equations (that is, extrapolated from data), the K_d values are defined as follows:

$$K_d = \frac{\text{Concentration } ^{233}\text{U absorbed onto bone char}}{\text{Concentration residual activity } (^{233}\text{U}) \text{ in liquid}}$$

$$K_d = \frac{x/m}{C} \quad .$$

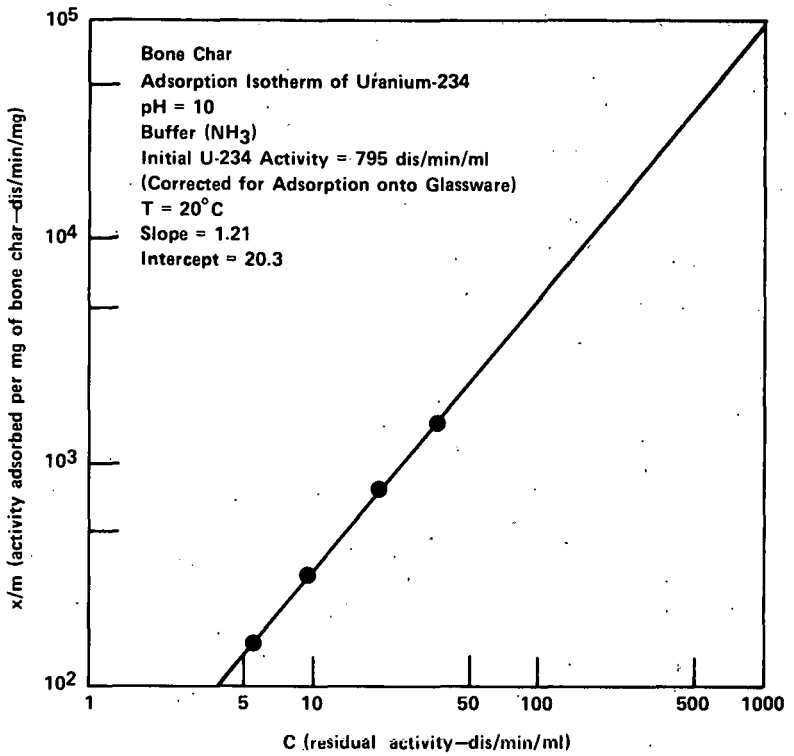

FIGURE 20 - Adsorption of uranium onto bone char at pH 10.

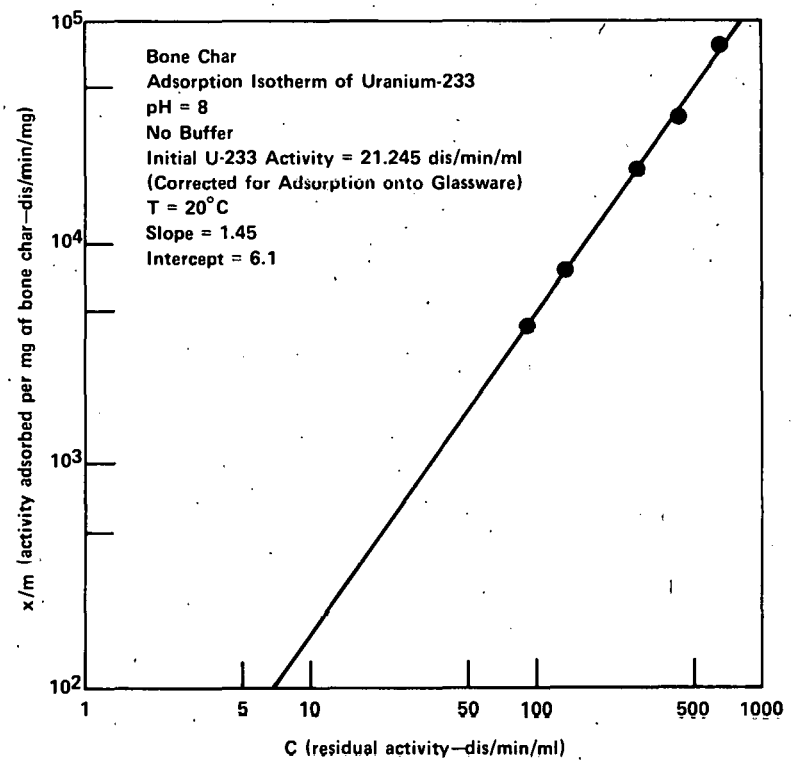

FIGURE 21 - Adsorption of uranium onto bone char at pH 8.

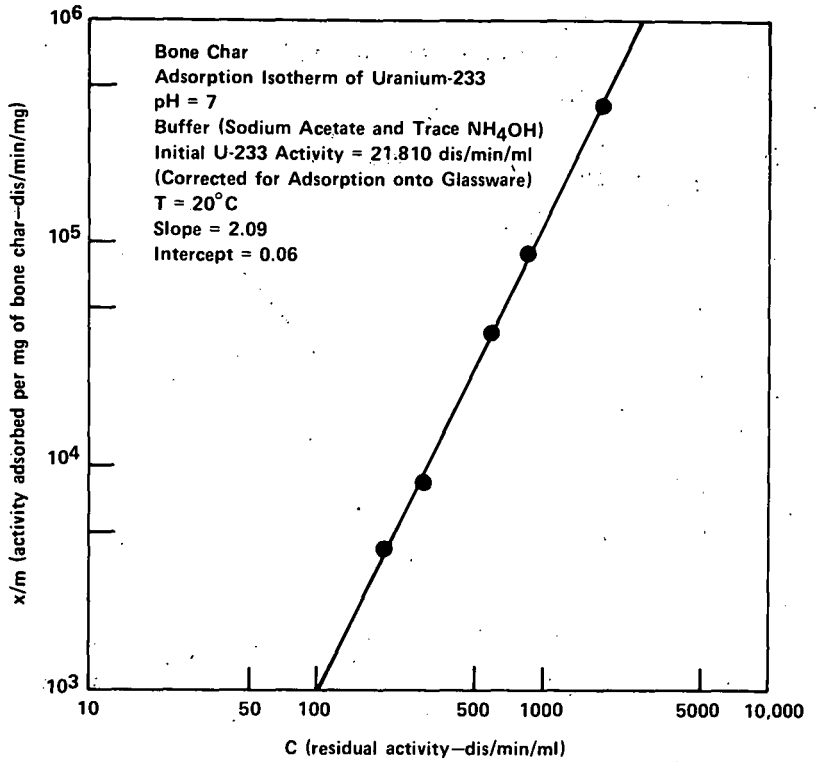

FIGURE 22 - Adsorption of uranium onto bone char at pH 7.

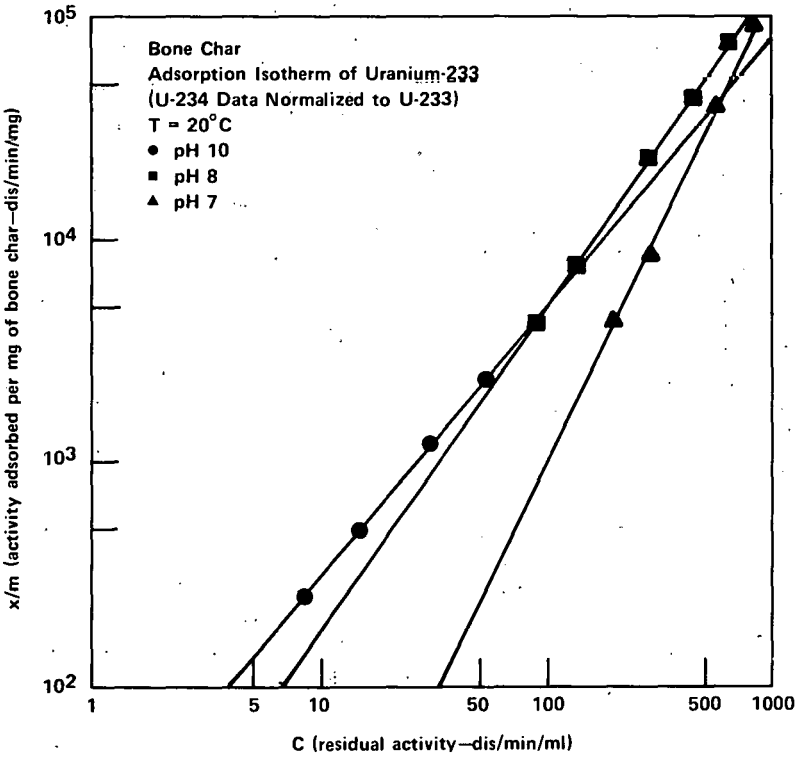

FIGURE 23 - Comparison of adsorption of uranium onto bone char at various pH values.

The values of concentrations used in the extrapolations ranged from 1 to 500 dis/min/ml ^{233}U, which is equivalent to 2.25×10^{-10} $\frac{\text{gram mole}}{\text{liter}}$ to 1.1×10^{-7} $\frac{\text{gram mole}}{\text{liter}}$. The K_d values were then plotted versus residual concentration (that is, the concentration in equilibrium with the bone char) of uranium to determine the effect of pH on the distribution coefficients (see Figure 24). As one can readily ascertain, the steepest slope occurs at pH 7. At low values of C, the higher K_d values occur at pH 10. This graph is similar to Figure 23 since the data in Figure 23 were used to generate Figure 24. However, it is easier to visualize the behavior of uranium when one looks at Figure 24. Three possible mechanisms could cause this behavior. The first possible explanation is that of polymer formation, and uranium has the following forms:

1) UO_2^{+2}

2) $(UO_2)_2 (OH)_2^{+2}$ - Dimer

3) $(UO_2)_3 (OH)_5^{+}$ - Trimer

As the pH is increased, the formation of dimer and trimer occur more readily. Since the mechanism of removal is thought to be chemisorption at pH 10, where it is thought that dimer and trimer would exist, more uranium would be removed per unit valence reacting with the surface. Therefore, high initial K_d values are apparent at pH 10 and the change in K_d with C is not as drastic as at pH 7. At pH 7, the initial K_d values are quite low, as compared to pH 10; however, the K_d changes vary rapidly with C, which is indicative of polymer formation.

The second possible explanation is that of complex formation. Since the commercial bone char is relatively impure, a number of possible complexing agents could be dissolving from the bone char. These include PO_4^{-3} and CO_3^{-2} and many others. K_d was defined as the ratio of uranium adsorbed onto the bone char to the uranium in solution:

$$\frac{\left[UO_2^{+2}\right]_{\text{solid}}}{\left[UO_2^{+2}\right]_{\text{liquid}}} ;$$

however, if complexing agents are present:

$$K_d = \frac{[\text{uranium}]\ \text{solid}}{\left[UO_2^{+2}\right] + \left[U^*\right]} ,$$

where the U* is a uranium complex. Now then, if the uranium complex is inhibited from adsorbing onto the bone char surface, the results obtained would be similar to that seen in Figure 24, where the concentration of uranium complex is a function of pH.

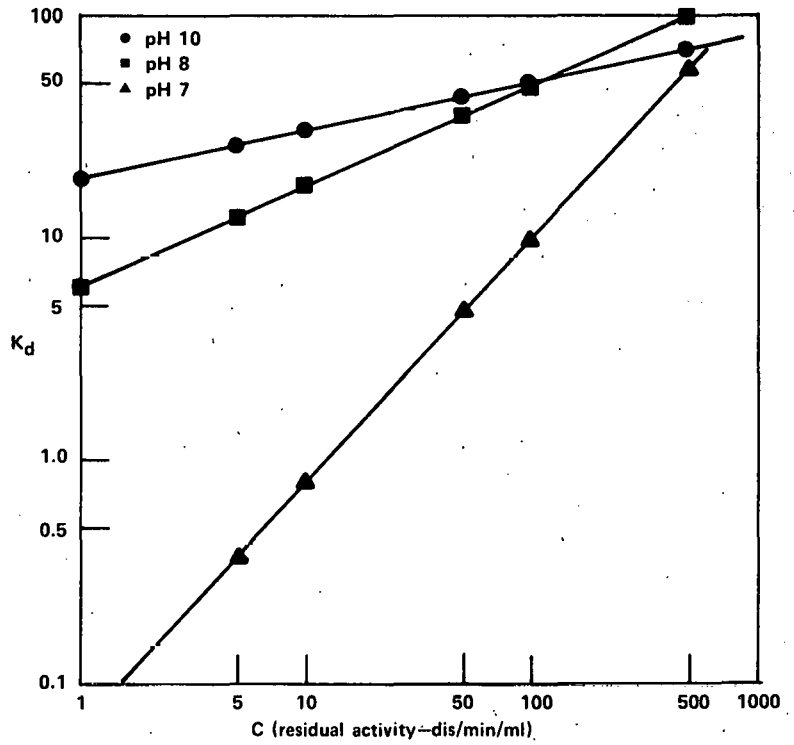

FIGURE 24 - Comparison of the distribution coefficient (K_d) with concentration (C) at various pH values.

The third possible explanation is that the surface becomes activated for adsorption as a function of pH. This could be caused by a heterogeneous surface activation energy, which is also the basis for the derivation of the Freundlich model for adsorption. This type of behavior is better observed when the data is plotted in the form of Figure 25 where the distribution coefficient (K_d) is plotted as a function of sorbent loading (x/m) for the various pH's studied. The curve for pH exhibits a low K_d for low sorbent loadings; however, after an initial loading the K_d values increase rapidly until a new value for x/m is reached whereupon the K_d changes only slightly. At pH 8, the K_d curve exhibits only slight curvature; and at pH 10 it is a straight line on a log-log plot. Therefore, if there is a surface phenomenon it occurs mostly at pH less than 8. This surface phenomenon could of course be attributed to a dissolution of the bone char surface at pH less than 8 that would affect the magnitude of the K_d values in the manner described in Figure 25.

At this time, it is difficult to distinguish between the three possible explanations for the behavior of uranium adsorption onto bone char. Further studies will be made to evaluate these three mechanisms and determine the behavior of uranium in this type of system. *(J. Koenst)*

THORIUM-229

A total of 17.68 mg ^{229}Th has been extracted and purified during this report period from aged ^{233}U. Of this quantity, 6.64 mg were extracted from unprocessed ^{233}U and the remainder, 11.04 mg, was extracted from previously processed ^{233}U.

The first batch processed consisted of two portions of ^{233}U oxide that were combined after extracting the ^{233}U. The resulting 2N HNO_3 solution of ^{229}Th and daughters was concentrated to 8N HNO_3 and passed through the anion exchange resin column. The product solution of 6.64 mg ^{229}Th was calculated to be 6% pure in ^{229}Th. The purity is an estimate because of weighing an uncertain form of the final product; it is assumed to be $Th(NO_3)_4 \cdot 12H_2O$.

The second batch also consisted of two portions of ^{233}U oxide. However, this material was much higher in ^{232}U than previously processed, 17 ppm versus 2-7 ppm for all other material processed in the past. Gamma radiation was higher by several orders of magnitude. This material was the second batch processed for the second time. This also should result in a product low in ^{232}Th. The final product was 8.19 mg ^{229}Th with a purity of 74%.

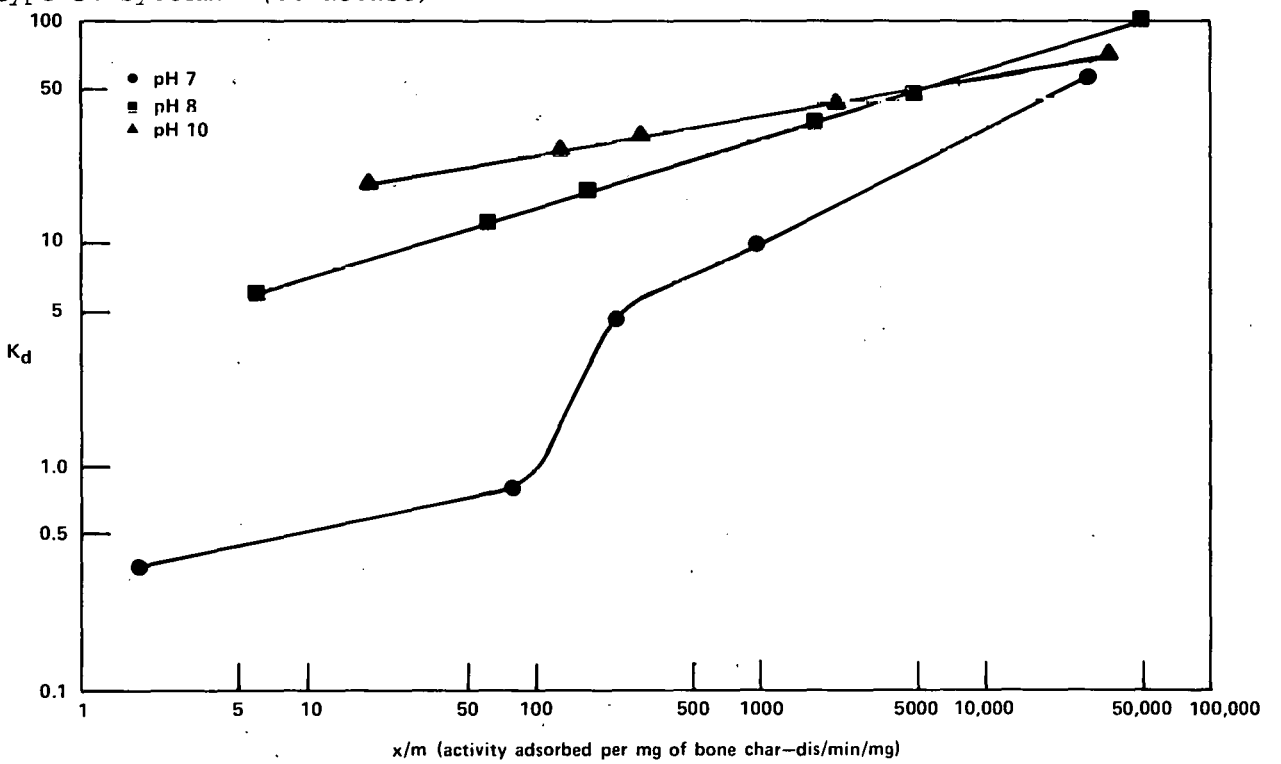

FIGURE 25 - Comparison of the distribution coefficient (K_d) with loading of the sorbent (x/m) at various pH values.

Some product material produced earlier, 1.68 mg ^{229}Th, appeared to be highly contaminated, which would give low product values and low total purity. This material had been purified by solvent extraction with TOPO. This was dissolved, filtered, adjusted to 8N HNO_3 and passed through the anion exchange column. The final product was much cleaner in appearance and assayed to have 2.85 mg ^{229}Th with a purity of 59%.

An anion exchange resin used for the final purification and concentration of ^{229}Th, will be used for all subsequent $^{233}U/^{229}Th$ processing. It provides for closer control over the product purity by the use of alpha pulse height analysis of individual fractions. Also, the resin column acts as a filter to remove solids and organic impurities from the product stream.

The procedure is as follows:

1. After the ^{233}U has been extracted from the 2N HNO_3 feed solution, separate the organic from the aqueous phase. Wash with di-ethyl-benzene to reduce any remaining DSBPP to a minimum.
2. Concentrate the ^{229}Th rich solution to 8N HNO_3. Filter through a coarse filter.
3. Prepare anion exchange resin AG 1X8 100-200 mesh by treating with 8N HNO_3 until chloride free. The column used was a 10 ml buret, 20 cm long, fitted with a 50 ml reservoir. The resin column was 16 cm x 0.5 cm. Flow was 0.3 ml/min.
4. Pass feed solution through column. If flow ceases, rod out column using a small diameter stainless steel rod.
5. Analyze raffinate for presence of ^{233}U.
6. Wash with 20 ml 8N HNO_3. Elute ^{229}Th with 50-100 ml 1N HNO_3. Analyze fractions until all ^{229}Th has been eluted. Any residual ^{229}Th may be recovered for future purification by igniting the resin. This should be done with caution because of the possible reaction between the organic resin and the acid.
7. Sample the product solution and analyze by scintillation counting and alpha pulse height analysis. *(W. S. Stringham)*

URANIUM-234

Mound Laboratory has been separating and recovering high isotopic purity uranium-234 from aged plutonium-238 materials for several years. The chemical procedures for separating and purifying the uranium have been described previously.[37]

Final purification of ^{234}U product A13-2 was described in the last report,[38] but the analyses were still in progress. Total oxide weight of 22.285 g was reported with a mass analysis indicating 99.08% ^{234}U, 0.08% ^{235}U, 0.06% ^{236}U, and 0.79% ^{238}U with some mass 237 observed.

Completion of impurity analysis by emission spectroscopy indicated 1.44% total impurities with iron and sodium the major impurities at 0.4% and 0.5%, respectively. Other impurities detected were bismuth, silicon, magnesium, lead, chromium, nickel, aluminum, copper, and molybdenum. Uranium-234 content calculated from mass analysis data and oxide weight corrected for impurities was 18.406 g. Alpha pulse height analysis of several samples indicated a ^{238}Pu content as high as 27 ppm. This ^{238}Pu content was in sharp disagreement with analyses of the nine solutions from which the uranium product was precipitated. The uranium content of these solutions contained only 1-2 ppm ^{238}Pu. Since the uranium from these nine solutions was precipitated in seven individual precipitations and calcined independently, the conclusion was that some source of ^{238}Pu contamination had made the product nonhomogeneous with respect to ^{238}Pu.

Using the available alpha pulse height data, a calorimetric measurement of the total product and the ^{234}U weight determined from mass analysis data, a ^{238}Pu content of 3 ppm was calculated for the product. Final alpha pulse height analysis (6/6/75) was reported as follows:

^{234}U = 90.51%

^{232}U = 7.52% (25 ppm on weight basis)

^{238}Pu = 0.81% (3 ppm on weight basis)

Other = 1.16% (daughters of ^{232}U)

Shipment of ^{234}U product A13-2 (18.406g) was made to the Heavy Element Pool at Oak Ridge National Laboratory on June 18, 1975.

As reported previously,[38] approximately seven grams of ^{234}U did not load onto the resin during the final anion exchange of product A13-2 and was distributed through the raffinate, wash, and neptunium fractions. There was a possibility that this uranium formed a phosphite compound because H_3PO_2 is used as a stabilizer in HI, which was used as a reductant for the ^{238}Pu. In fact, there is a method reported[39] that separates uranium from plutonium by a homogeneous precipitation of uranium with H_3PO_2. This method separates uranium (+4) from plutonium (+3), using HI as the source of H_3PO_2. One of the wash fractions containing about 43 mg

^{234}U and less than 1 mg ^{238}Pu was selected to investigate the use of this method for separation of ^{234}U. For this investigation, H_3PO_3 was used as the precipitating agent with Na_2SO_3 to reduce the uranium to the +4 state and ferrous sulfamate to reduce the plutonium to the +3 state. No precipitation of uranyl phosphite was achieved, apparently because of the presence of phosphate in the solution. Free iodine remaining in the solution had probably oxidized any phosphite formed during the anion exchange processing. This precipitation is reported not to work in the presence of phosphate. The method should be investigated in the future with uranyl chloride known to be free of iodine or phosphate.

The recoverable uranium and plutonium remaining in the raffinate, wash, and neptunium fractions from the final anion exchange of product Al3-2 were precipitated as hydroxides to separate any free iodine and phosphate. The precipitate was dissolved in concentrated HCl, which was adjusted to 9M HCl, and is being held for reprocessing through the final anion exchange. Ammonium iodide will be tried in place of HI as a reductant for the plutonium during this anion exchange in the future.

Solution Al0-P, containing an estimated four grams of ^{234}U and 11.4 g of ^{238}Pu in high acid concentration, was obtained from dissolution of Pu-Zr heat source material several years ago. It has been evaporated to near dryness, redissolved in concentrated HNO_3, and adjusted to 2M HNO_3 in preparation for the initial purification step, namely, oxalate precipitation of the ^{238}Pu.

Solution U-8, containing an estimated one gram of ^{234}U and 0.2 g of ^{238}Pu in high acid concentration, was concentrated several years ago by solvent extraction from waste solutions obtained from plutonium recovery operations. This solution has been evaporated to near dryness, the solids redissolved in concentrated HNO_3, and adjusted to 0.3M HNO_3 in preparation for the intermediate purification step, namely, anion exchange in nitrate media using $Al(NO)_3$ as the salting agent. Similar solutions U-9 and U-10 are being adjusted to 0.3M HNO_3 by precipitation of the uranium and plutonium with NH_4OH and dissolution of the precipitate in HNO_3. Evaporation to near dryness proved too "touchy" for these solutions; the cooling solids cracked the Pyrex evaporator when working with U-8.

The receipt of approximately 100 liters of waste solution from plutonium recovery operations was reported last year.[40] These solutions were designated "evaporator concentrate" (10 liters) and "^{234}U raffinates" (96 liters) and contained an estimated 65 g of ^{234}U and 32 g ^{238}Pu. Several methods of preliminary concentration were investigated at that time, but the space limitations in the ^{234}U production area made processing of such a large volume impractical. Recently, the larger scaled equipment of plutonium recovery operations became available for use. These solutions were transferred to that area, combined as "U-raffinates" and concentrated by anion exchange. Four runs were required to process the solution. The solution was salted with $Al(NO_3)_3$ to 1.6M, adjusted to 0.3M HNO_3, and fed through the column of Dowex 1 x 4 resin to load both uranium and plutonium. Uranium and plutonium were eluted together with 0.35M HNO_3 and 0.35M hydroxylamine nitrate (to reduce plutonium). The raffinates, containing most of the impurities, were discarded and the eluants evaporated to a minimum volume. The plutonium in the eluants was precipitated as the oxlate with oxalic acid, and the uranium-rich filtrate was evaporated to a volume of approximately eight liters. This filtrate, containing five grams of ^{238}Pu, is now ready to be prepared as feed to the intermediate purification step in the ^{234}U production area. If the estimated uranium content proves to be correct, processing of this filtrate will require two to three years.
(P. L. Keister)

CALCIUM ISOTOPE SEPARATION

Chemical Exchange

A prototype chemical exchange system using a Karr, reciprocating-plate, countercurrent, extraction column, and reflux equipment was operated at total reflux for an extended period to enrich calcium isotopes. The polyether dicyclohexyl 18-crown-6 was used for the calcium isotope exchange reaction. The formation of the calcium complex in the top reflux system was estimated to be only one-fourth complete based upon equilibrium distributions between the organic phase and the aqueous phase. This made it necessary to supply low throughputs to the column, and, consequently, axial backmixing became a substantial factor in reducing the column separation factor. A new contacter design is being planned to alleviate this situation.
(R. W. Hurd)

LIQUID THERMAL DIFFUSION

Liquid thermal diffusion is being developed as a general technique for separating stable isotopes. It has been established that liquid phase isotopic thermal diffusion factors are large enough for separation on a practical scale.[41] Several types of prototype columns have been constructed and tested. Columns of the most recently developed design have been found to perform consistently in accordance with theoretical predictions.

Sulfur Isotope Separation

The previous report in this series[42] described the separation of highly enriched sulfur-34 (natural abundance: 4.2%) in a 12 column dual cascade. At that time, the desired concentration of 90% ^{34}S had been reached and withdrawal of product had been established at 2.0 g of CS_2 per week, equivalent to approximately 1.5 g of ^{34}S per week.

Production of ^{34}S continued, with interruptions, until September 22, 1975. At that time, sufficient material and data had been acquired; and the experiment was terminated.

Figure 26 is a plot of product concentration and flow rate during the production period. Production was suspended for a time when the concentration of ^{34}S dropped below 90%. The drop was the result of plugging of the column cooling water distributors by particulate matter. The associated temperature asymmetry caused a large decrease in the separation efficiency of the affected columns.

Several steps were taken to avoid future difficulties with the cooling water. A screen filter was installed in the system water supply, and the column water distributors were redesigned to trap particles at the inlet.

Control of the flow of depleted CS_2 from the top of the cascade was found to be difficult. Several devices were tried, including a syringe pump and a capillary leak; but a satisfactory, high level of reliability could not be obtained. These were finally abandoned in favor of a nominal 500 ml reservoir at the top of the system. The reservoir was periodically changed as the ^{34}S content was depleted.

Table 9 contains the transport data acquired over several complete cycles of depletion and replacement of the feed reservoir. The equivalent transport rates of ^{34}S were calculated from:

$$\tau = \frac{64}{76} (w_o - w) W_R / \Delta t, \qquad (1)$$

where w_o and w are the initial and final ^{34}S concentrations, W_R is the CS_2 content of the reservoir, and Δt is the time span. The cascade calculations predict a transport rate of 0.81 g/day at the time the desired concentration of 90% ^{34}S is reached.

It appears that the transport rate was approximately 50% of that predicted from theory. There are several possible reasons for this, the most likely being that the initial transport coefficient H was somewhat lower than predicted. The initial transport coefficient is proportional to the square of the temperature difference between the hot and cold walls of the column; thus, a relatively modest error in estimating the wall temperatures could account for the low result. The wall temperatures differ by 20 to 40°C from the respective steam and cooling water temperatures, and estimates of these temperature drops are not especially reliable.

Table 9

TRANSPORT DATA FOR THE TOP RESERVOIR[a] OF THE SULFUR THERMAL DIFFUSION CASCADE

Cycle	Time, Days	^{34}S, %	Transport Rate g/day ^{34}S
1	0	4.24	
	7.93	3.75	
	13.68	3.54	0.28
2	0	4.24	
	13.13	3.30	0.39
3	0	4.24	
	7.12	3.58	
	16.95	3.07	0.38

[a]Reservoir Content: 649 g CS^2

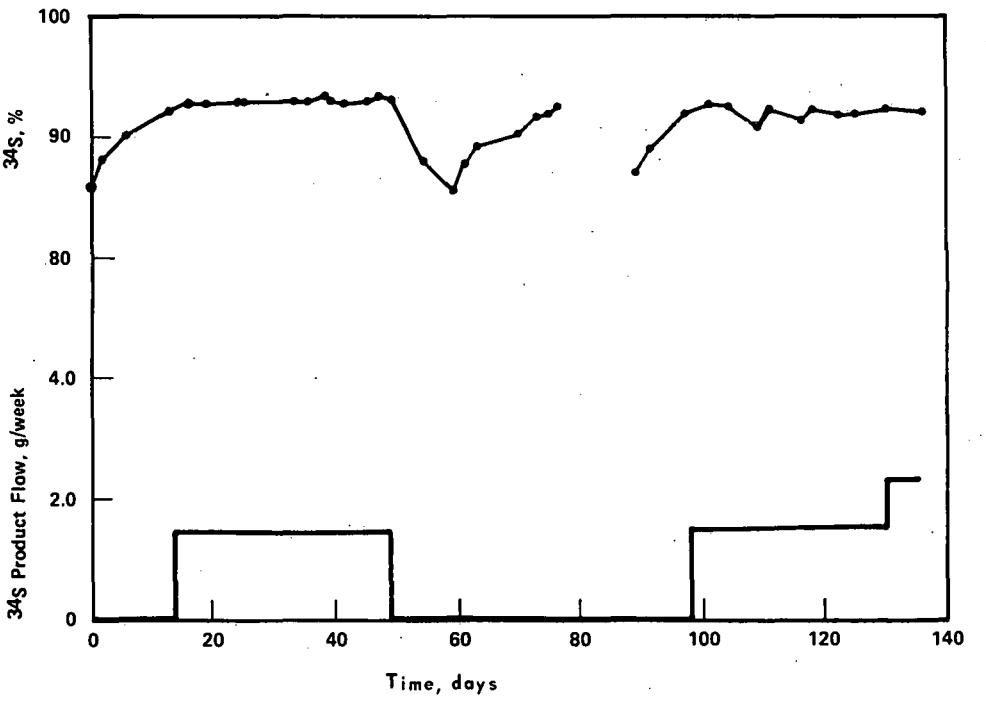

FIGURE 26 - Performance of the 12-column liquid thermal diffusion cascade for sulfur-34 enrichment.

At the conclusion of the ^{34}S separation experiment, additional material of greater than 90% enrichment was recovered from the last stage of the cascade. When this material was added to the material previously produced, the total was equivalent to 20.0 g of ^{34}S. *(W. M. Rutherford)*

Chlorine Isotope Separation

In previous work, two chlorine compounds, 1-chloropropane and chlorobenzene were considered as fluids for chlorine isotope separation. Separation measurements were completed for both compounds in the 60 cm research column. It was found that the isotopic thermal diffusion factor of 1-chloropropane was nearly the same as that of chlorobenzene. Chlorobenzene, however, because of its physical properties yielded a somewhat higher separation factor.

Additional experiments with these two compounds were recently completed in a 60 cm prototype column. The separation of the two chlorine isotopes, ^{35}Cl and ^{37}Cl, was measured as a function of time. Column parameters were derived from the data by fitting to the solution of the differential equation describing the transient performance of the column:

$$\frac{\partial w_1}{\partial t} = -\frac{1}{\mu}\frac{\partial}{\partial z}\left[Hw_1(1-w_1) - K\frac{\partial w_1}{\partial z}\right], \qquad (2)$$

where w_1 is the mass fraction of component 1, t is the time, μ is the holdup per unit length, and z is the vertical coordinate. The quantities H and K are the initial transport coefficient and the remixing coefficient, respectively. According to Eq. 2, the separation at infinite time is given by:

$$\ell n q_e = HL/K$$

where L is the length of the column and the separation factor q_e is defined by:

$$q_e = \frac{w_{1B}(1-w_1)_T}{w_{1T}(1-w_1)_B}. \qquad (3)$$

The subscripts T and B refer to the top and bottom ends of the column, respectively.

Table 10 gives the results of the recent experiments with the prototype column along with those obtained earlier with the 60 cm research column.[43]

The results are not entirely consistent. The value of $\ell n q_e$ for chlorobenzene was higher in the prototype than in the research column. The opposite was the case for 1-chloropropane. According to theory, the same compound should yield the same value in each of the two columns. If one of the two columns had been subject to parasitic effects, then the values for both compounds should deviate in the same direction.

The data from the prototype show that the initial transport coefficient H is significantly larger for 1-chloropropane than for chlorobenzene. Again, the data show an inconsistency. The value of H in the prototype column should be greater than that in the research column by a factor of 4/3, according to the ratios of the annular diameters; however, the measured value is somewhat smaller. The initial transport coefficient was not measured for chlorobenzene in the 60 cm research column.

A consideration of the above data and the characteristics of the several available thermal diffusion columns led to the choice of 1-chloropropane as the working fluid for the first experiment on the separation of highly enriched chlorine isotopes. The available columns were those used in the sulfur-34 separation experiment plus four additional new columns. This provided more than sufficient length to offset the low observed value of $\ell n q_e$ for chloropropane. The higher value of H combined with the lower molecular weight of 1-chloropropane promised a much higher chlorine isotope transport rate than that which could be obtained with chlorobenzene.

Following the shutdown of the sulfur-34 separation experiment, a cascade of 16 columns in series was assembled for the chlorine separation experiment. The dimensions and parameters of the columns are given in Table 11. The column coefficients reported in Table 11 were derived from the values measured for the 60 cm prototype column by means of the following relationships:

$$\ell n q_e = (\ell n q_e)_o\,(a_o/a)^4\,(L/L_o) \qquad (4)$$

$$H = (H)_o\,(a/a_o)^3\,(d/d_o), \qquad (5)$$

where a is the spacing between the hot and cold walls, d is the diameter of the annulus and the subscript $_o$ refers to the data for the 60 cm prototype as reported in Table 10.

Before the cascade was started up, it was necessary to remove columns 4 and 5 for major repairs. Thus, the cascade was started on October 21, 1975, as a 14 column cascade.

The concentration of chlorine-37 in the bottom of the 14-column cascade as a function of time is plotted in Figure 27.

Table 10

COLUMN PARAMETERS FOR CHLORINE ISOTOPE SEPARATION

	60 cm prototype column	60 cm research column
mean annular diameter	25.3 mm	18.8 mm
gap	254 μm	254 μm
ℓnq_e, chlorobenzene	0.65	0.53
ℓnq_e, 1-chloropropane	0.34	0.46
H, chlorobenzene	2.5×10^{-5} g/sec	---
H, 1-chloropropane	4.0×10^{-5}	4.6×10^{-5} g/sec

Also plotted in Figure 27 is a curve calculated from theory for the 14 column system using the column coefficients given in Table 11. The predicted curve is followed reasonably well up to the sixth day. After that, the progress of the separation was delayed by a series of experimental misfortunes (leaks, plugged lines, malfunctioning circulating pumps, etc.); but it is expected that these will be overcome in due course. *(W. M. Rutherford and E. D. Michaels)*

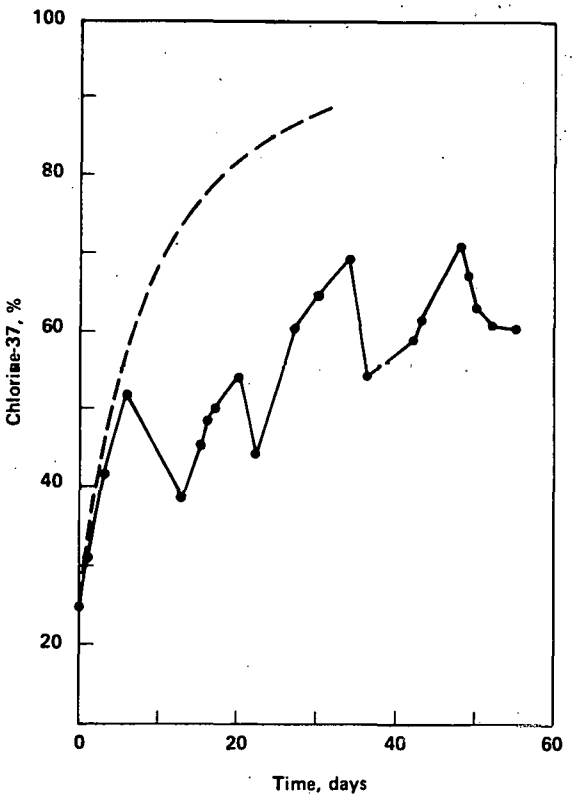

FIGURE 27 - Chlorine-37 concentration at the bottom of the 14-column liquid thermal diffusion cascade. The dashed line is calculated from theory.

MOLECULAR BEAM SCATTERING

Total Scattering Cross Sections

The current series of argon-krypton total scattering cross section experiments is being run over a relative kinetic energy range that covers three different regions. The first (and highest) energy region used a room temperature target and varying source temperatures from 375 K down to 120 K with LN_2 cooling. The second region uses the Cryo-tip refrigerator to cool the source from 120 K to 75 K, still using a room temperature target. The third and final region uses expansion-cooled nitrogen gas to lower the target temperature to 130 K and the Cryo-tip for source cooling to 75 K. This series will thereby give total cross section measurements for argon-krypton scattering over the relative velocity range between 3.29×10^4 and 6.83×10^4 cm/sec (relative kinetic energies between 2.5×10^{-14} and 1.0×10^{-13} erg).

Table 11

PARAMETERS FOR CHLORINE ISOTOPE SEPARATION IN A 16 COLUMN LIQUID THERMAL DIFFUSION CASCADE USING 1-CHLOROPROPANE AS THE WORKING FLUID

Column	Length, m	Gap, mm	Mean annular diameter, mm	10 H, g/sec	&nqe
1	0.76	254	25.3	2.7	0.43
2	0.76	254	25.3	2.7	0.43
3	0.76	254	25.3	2.7	0.43
4	2.4	305	25.3	4.6	0.66
5	2.4	305	25.3	4.6	0.66
6	2.4	305	25.3	4.6	0.66
7	0.76	254	25.3	2.7	0.43
8	0.76	254	25.3	2.7	0.43
9	0.76	254	25.3	2.7	0.43
10	0.76	254	25.3	2.7	0.43
11	0.76	254	25.3	2.7	0.43
12	0.76	254	25.3	2.7	0.43
13	0.76	254	25.3	2.7	0.43
14	0.76	254	25.3	2.7	0.43
15	0.60	254	18.8	2.0	0.34
16	0.91	178	18.8	0.7	2.12

Experiments in the first two regions of this argon-krypton series have been completed. Table 12 gives a summary of the reduced experimental data from these experiments. Several discrepancies have been found in the data reduction methods used earlier that caused some errors in the previously reported results.[44] These have been corrected and are included here along with recent data for all argon-krypton experiments to date. The relative velocity cross section is given by:

$$Q(v_r) = \frac{Q_e}{Fa_o(6,x)} \left(\frac{v_b}{v_r}\right)^{\frac{2}{5}},$$

where Q_e is the measured effective cross section described earlier,[45] and $Fa_o(6,x)$ is the Berkling[46] correction function that assumes a Maxwellian target velocity distribution and a monochromatic beam. Previous calculations used the Berkling G series correction functions, which assumed a Maxwellian velocity distribution in both the beam and target.[45] Since we are using a supersonic nozzle beam with less than a 10% half-intensity-width, the assumption of monochromaticity is more appropriate than a Maxwellian velocity distribution for the beam. The average relative velocity is given by:

$$v_r = (v_b^2 + v_t^2)^{\frac{1}{2}},$$

where v_b is the most probable beam velocity, and v_t is the average target velocity. The quantities T_s and T_t are the beam source and target temperatures, respectively.

A second correction involves the effective path length that the primary beam encounters in passing through the scattering cell. In the previous calculations, the outside diameter of the cell was a assumed to be the path length; however, this is not strictly correct because, as will be shown, the effective path length, L_{eff}, is somewhat less than the outside diameter of the tube. The situation is as shown in Figure 28.

There is a resistance to flow out of the circular orifices that consist of a resistance caused by the orifice opening (Z_o) and that through the passages in the wall (Z_{LW}).

$$Z_o = \frac{16}{\pi} \cdot \frac{1}{\bar{v}d^2}$$

$$Z_{LW} = \frac{12}{\pi} \frac{1}{\bar{v}} \cdot \frac{L_N}{d^3}$$

where d is the diameter of the opening, $\bar{v}$ is the molecular velocity, and L_W is the wall thickness.

$$Zg_1 = Zg_2 = Z_o + Z_{LW}$$

$$Zg_1 = \frac{4}{\pi} \frac{1}{\bar{v}} \frac{1}{d^2} \left[4 + \frac{3LW}{d}\right]$$

Now, the scattering zone can be thought of as the region through which the beam passes where there are finite pressures, for example, the inside of the cell and the two canals inside the walls. The boundary condition is that P = 0 immediately outside of the outer wall.

The pressure drops in a fashion inversely proportional to the flow from the chamber past a given point. In otherwords, the pressure established at a given incremental length of channel is equal to the fraction of the total resistance encountered in that region times the initial pressure. Therefore,

$$P_o = \frac{Z_o}{Zg_1} \cdot P_k \text{ and } P_{LW} = \frac{Z_{LW}}{Zg_1} \cdot P_c$$

and similarly for Zg_2.

The effective length is defined as that length which, when multiplied by the known cell pressure (p_c), would be equivalent to the sum of all actual lengths times actual pressures. Let L_c be the actual inside diameter of the cell, then

$$p_c L_{eff} = (P_{LW/2}) \cdot LW + p_c L_c + (P_{LW/2}) \cdot L_W$$

$$= \frac{Z_{LW}}{Zg_1} L_W p_c + p_c L_c$$

From this it follows that

$$L_{eff} = \frac{L_W^2}{4/3d + L_W} + L_c,$$

which for the actual dimension given in Figure 28 yields L_{eff} = 1.14 cm.

A third procedural change involves the data points used in determining the cross section from the beam intensity attenuation vs. target cell gas density. The relationship between the incident (I_o) and transmitted (I) beam is assumed to follow Beer's law, $I = I_o e^{-Qnl_{eff}}$, where n is the gas density in the target cell and Q is the effective cross section we are trying to measure. Q is determined from the slope of the $\ell n(I/I_o)$ vs. n plot as described in ref 44. Now if Beer's law is applicable, the plot must be a straight line through the origin. At higher densities multiple scattering occurs, and the plot is no longer linear. Originally, this experimental nonlinearity was thought to be scatter, and including these points in the least squares determination skewed the slope away from the origin. The procedural change is that these high density

Table 12

SUMMARY ARGON-KRYPTON AND KRYPTON-ARGON TOTAL CROSS SECTIONS

Scattered Pair	Experiment No.	Source Temperature (K)	Target Temperature (K)	$v_r \times 10^{-4}$ (cm/sec)	Q_e (Å²)	Fa_o (6,x)	$Q(v_r)$ (Å²)
Ar-Kr	TOT 22A	300	300	6.233	379.9	1.0465	364.0
Ar-Kr	TOT 22B	300	300	6.233	407.0	1.0465	372.0
Kr-Ar	TOT 25A	244	300	5.301	521.9	1.2434	354.7
Kr-Ar	TOT 25B	244	300	5.301	559.5	1.2434	380.2
Kr-Ar	TOT 27A	244	300	5.301	556.1	1.2434	377.9
Kr-Ar	TOT 27B	244	300	5.301	536.3	1.2434	364.5
Ar-Kr	TOT 26A	196	300	5.294	484.3	1.0718	424.1
Ar-Kr	TOT 26B	196	300	5.294	480.6	1.0718	420.8
Ar-Kr	TOT 24A	180	300	5.135	460.5	1.0782	398.9
Ar-Kr	TOT 24B	180	300	5.135	469.0	1.0782	406.3
Kr-Ar	TOT 23A	180	300	4.993	620.0	1.3141	384.2
Kr-Ar	TOT 23B	180	300	4.993	637.4	1.3141	395.0
Kr-Ar	TOT 29A	120	300	4.685	758.3	1.4309	408.2
Kr-Ar	TOT 29B	120	300	4.685	780.0	1.4309	419.9
Ar-Kr	TOT 28A	120	300	4.485	529.6	1.1178	430.7
Ar-Kr	TOT 28B	120	300	4.485	534.4	1.1178	434.6
Ar-Kr	TOT 30A	100	300	4.246	600.5	1.1407	471.7
Ar-Kr	TOT 30B	100	300	4.246	582.3	1.1407	457.3
Ar-Kr	TOT 31A	75	300	3.928	649.4	1.1851	478.2
Ar-Kr	TOT 31B	75	300	3.928	645.6	1.1851	475.3
Ar-Kr	TOT 32A	120	130	3.974	525.5	1.0504	477.4
Ar-Kr	TOT 32B	120	130	3.974	525.9	1.0504	477.7
Ar-Kr	TOT 33A	100	130	3.703	551.9	1.0560	494.5
Ar-Kr	TOT 33B	100	130	3.703	548.2	1.0560	491.2

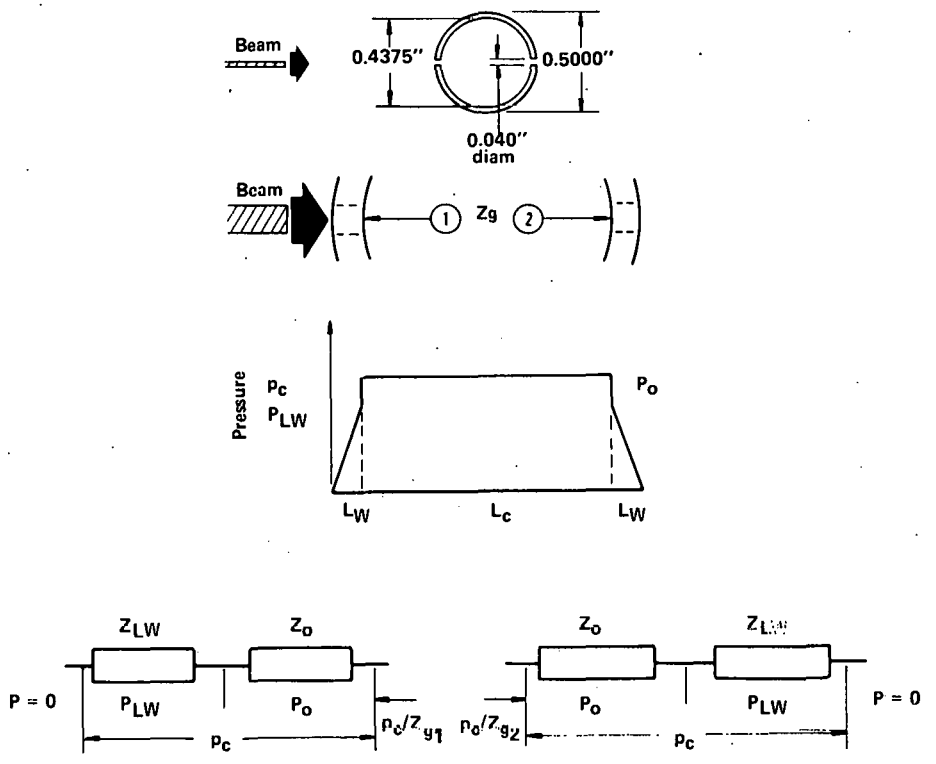

FIGURE 28 - Schematic of pressure drop and flow resistance in total cross section scattering cell.

points are discarded above the onset of nonlinearity, which has resulted in linear plots passing through the origin.

The only extensive total cross section measurements for the argon-krypton system found in the literature have recently been reported by Bredewout.[47] His measurements cover the higher energy collision systems with relative velocities above 5.34×10^4 cm/sec. Rothe and Neynaber some time ago reported argon-krypton data for a single relative velocity of 4.85×10^4 cm/sec. The present work overlaps these results with good agreement and extends the measurements into a lower energy range. Figure 29 shows the results obtained to date of the present work along with the aforementioned higher energy results. Experiments to obtain the data at the low end of the range are currently being conducted.

The quantum scattering computer program written earlier[49] has been rewritten to increase its versatility and to make necessary modifications for compatibility with our new in-house ModComp IV (Modular Computer Systems Inc.) computer. It is now possible to calculate any of the following theoretical quantities:

1. Quantum phase shifts - using the WKB approximation with any desired intermolecular potential form.
2. Differential scattering cross sections-both monochromatic and velocity averaged.
3. Total scattering cross sections.

This program has just been made operational and was used for its trial run to calculate the theoretical total cross sections for argon-krypton using the Lennard-Jones (12,6) potential. The subroutine for the potential was already written and, therefore, convenient to use for program testing. The curve that was generated from this calculation is shown in Figure 29 merely for reference, since it obviously does not provide a good theoretical correlation for the argon-krypton scattering system. Subroutines for other parametric potential models can now be written and substituted in the program with ease for best fit correlations to experimental data. *(R. W. York)*

Validity of "Semiclassical" Calculation

The theoretical curve shown in Figure 29 was calculated using the WKB approximation for the phase shifts with a Lennard-Jones (12-6) potential, followed by summation of

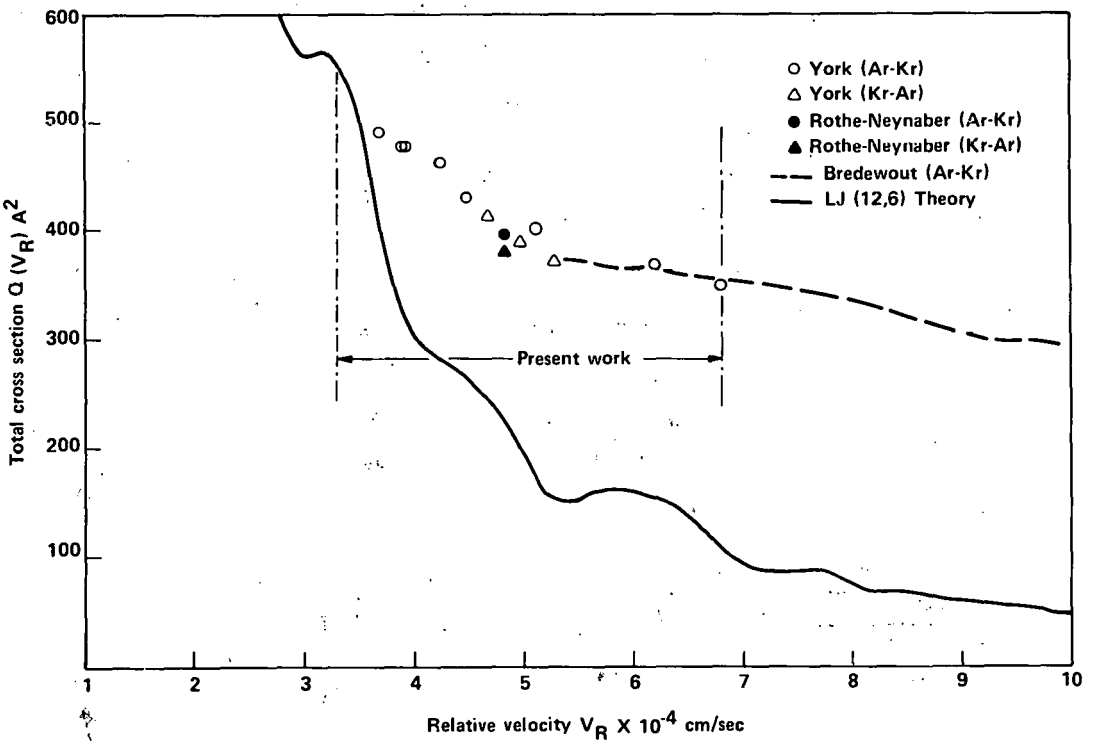

FIGURE 29 - Argon-Krypton total scattering cross sections.

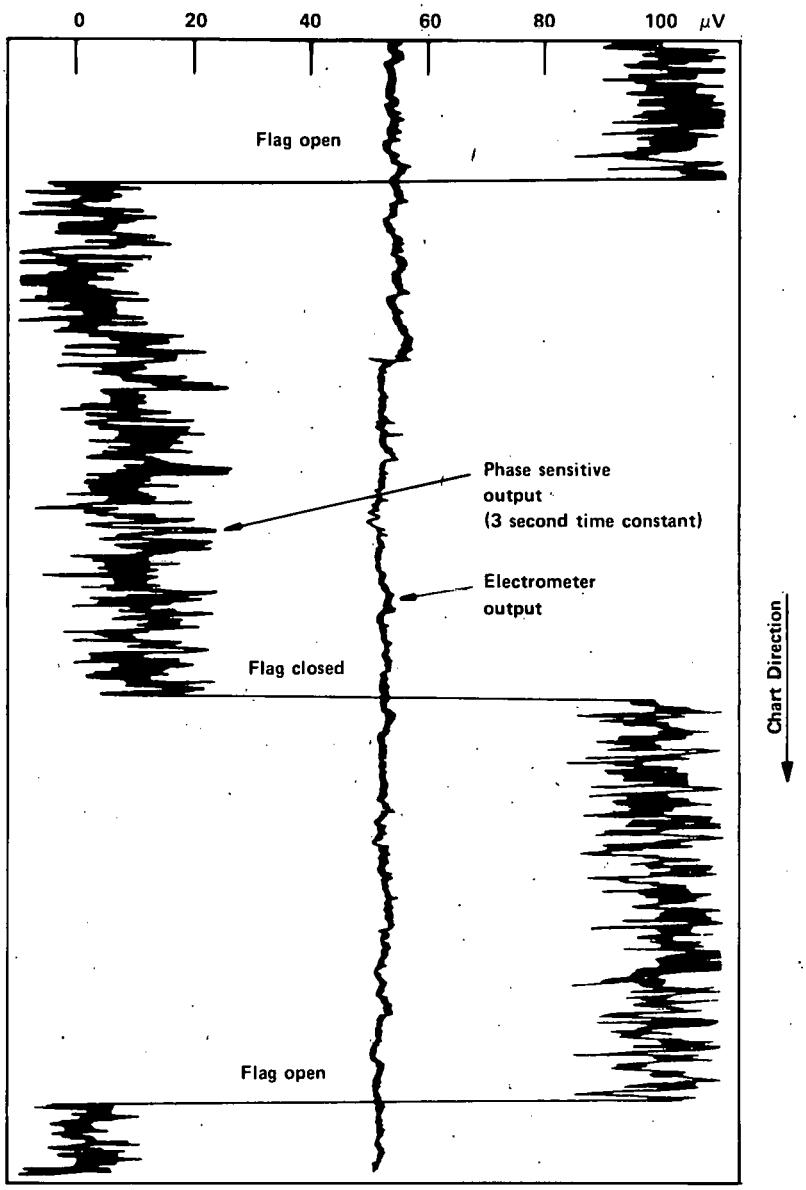

FIGURE 30 - Typical chart trace of the phase sensitive detector output.

the phase shifts to obtain the total cross sections. This is one variation of the so-called "semiclassical" method of calculating cross sections as opposed to a complete quantum mechanical treatment. One then should certainly ask the question as to whether the domain of validity of the approximation corresponds to that in which it is being compared with the experimental data. In order to check the validity of the approximation, however, one would have to perform the exact calculation in the first place, a rather formidable undertaking. Fortunately, Munn et al.[50] have done this and set forth criteria for establishing the domain of validity of the JWKB approximation for the LJ (12-6) potential, which is close enough for the present discussion. Using the criteria that when the discrepancy between the JWKB approximation and the exact calculation for the phase shift is greater than 0.05 radian, Munn et al. have plotted regions in the energy-angular momentum plane where the approximation is unsatisfactory (figure 2 in ref 7). The regions are plotted parametrically in the reduced de Broglie wavelength, Λ^*, and appear as loops in the E vs. ℓ diagram with the "fail" regions enclosed in the loops. Now the semiclassical approximations fail obviously at very low energies because they do not account for barrier penetration (tunneling), but they also fail up to rather surprisingly high energies because of a not-so-obvious phenomenon called partial reflection. The effective potential energy curve in a collision has a "hump", or barrier, which degenerates into a kink at higher values of the angular momentum (figure 3 in ref 7). The incoming particle-wave is partially reflected off this kink in a nonnegligible fashion to energies, which Munn et al. call the high energy edge and, which are determined by the maxima (along the energy axis) in the E vs. ℓ plane. Using their calculated values, Munn et al. demonstrated that the "max E" values from the loops were a straight line through the origin with slope 6.2 when E/ε was plotted versus (Λ^*) (figure 4 in ref 7). Thus, E (experimental) $\geq 6.2\ (\Lambda^*)^2$ is the criteria for checking the validity of the semiclassical approximations (strictly speaking, the JWKB) for any given system of reduced deBroglie wavelength Λ^*.

Using the LJ (12-6) potential parameters for argon and krypton in the usual combining rules for unlike interactions, one obtains ε/k = 153.5 K and σ = 3.514 Å for the Ar-Kr interactions. The reduced deBroglie wavelength is:

$$\Lambda^* = h/\sigma\,(2\mu\varepsilon)^{\frac{1}{2}}$$
$$= 0.137,$$

where μ is the reduced mass and h is Planck's constant. The lowest energy for which a curve is drawn in Figure 29 is E - 1.4×10^{-14} ergs, and the lowest E (experimental) is somewhat higher than this. The quantity $6.2\varepsilon(\Lambda^*)^2$ is equal to 0.25×10^{-14} so that the criteria of validity for use of the semiclassical approximation is met for the present work. *(W. L. Taylor)*

Molecular Beam Detection

Tests of the quadrupole molecular beam detector in the bell jar vacuum system have been concluded.[45] Using a tuning fork beam chopper, the phase-sensitive detector recorded a signal of around 100μV when the beam particle density of neon-20 at the ionizer was 1.6×10^9 particles/cm^3. The background partial pressure of neon-20 was estimated to be 1.0×10^{-5} torr. This corresponds to a particle density of 4×10^{11} particles/cm^3. The dc signal at the electrometer measuring this particle density was about one volt. The random noise level introduced to the phase-sensitive detector signal was around 10μV p-p when an integrated time constant of 10 sec was used. Figure 30 shows a typical chart trace of the detector output. A flag is used as a beam shutter. When the flag is closed, the output is near 0.0μV.

The random noise level measured by the phase sensitive detector, when no neon-20 is present in the chamber or when the quadrupole is detuned, is about 100 nV. Conclusions are that the quadrupole detector has the sensitivity and noise rejection capabilities needed for differential cross section measurements.

A rotary mount for the quadrupole detector has been constructed and tested. The quadrupole has been removed from the bell jar system and will be mounted in the beam chamber upon completion of the present cross section measurements. *(R. E. Miers)*

TRANSPORT PROPERTIES

Thermal Diffusion Factors for Ne-Ar, Ne-Kr, and Ar-Kr

As a continuation of the program to measure properties of binary mixtures of the noble gases, the thermal diffusion factors for Ne-Ar, Ne-Kr, and Ar-Kr were measured in the 20-tube trennschaukel. The composition dependence was determined at 250 K, and the α_T's for equimolar mixtures were measured as a function of temperature up to 750 K for each of the systems. The results are given in Tables 13 and 14.

Table 13

α_T FOR THE Ne-Ar SYSTEM AT 250 K

Run No.	X_1[a] (Feed)	T (corr.)	Corrections[b] A	B	C	Uncertainties[b] (±%) D	E	F	Dev. (%)
504	0.110	0.119	0.948	1.073	0.993	7.8	2.2	10.0	-2.7
502	0.353	0.146	0.951	1.073	0.993	4.4	0.8	5.2	4.0
511	0.498	0.157	0.977	1.060	0.992	3.9	0.7	4.6	1.9
503	0.653	0.160	0.950	1.073	0.993	1.0	1.6	2.6	-6.9
505	0.898	0.193	0.952	1.073	0.993	2.5	1.1	3.6	-8.1

α_T FOR THE Ne-Kr SYSTEM AT 250 K

510	0.103	0.195	0.966	1.057	0.994	3.4	1.4	4.8	0.4
508	0.353	0.212	0.965	1.056	0.994	0.7	2.2	2.9	-3.8
506	0.498	0.238	0.949	1.056	0.994	1.3	1.0	2.3	-0.4
520	0.498	0.246	0.949	1.056	0.994	1.1	2.8	3.9	3.0
507	0.655	0.274	0.966	1.056	0.994	1.0	1.3	2.3	4.2
509	0.897	0.279	0.955	1.048	0.995	1.5	1.1	2.6	-10.3
514	0.897	0.339	0.994	1.052	0.985	1.2	2.0	3.1	9.0

α_T FOR THE Ar-Kr SYSTEM AT 250 K

525	0.100	0.054	0.980	1.036	0.996	4.3	9.0	13.3	-1.4
524	0.100	0.055	0.978	1.036	0.996	7.1	2.0	9.1	0.4
516	0.100	0.055	0.972	1.060	0.992	6.3	1.7	8.0	0.4
512	0.301	0.055	0.918	1.028	0.997	6.6	1.0	7.6	-3.9
518	0.301	0.054	0.982	1.060	0.992	5.7	2.2	7.9	-5.7
523	0.305	0.062	0.979	1.036	0.996	11.4	1.9	13.3	8.2
521	0.501	0.063	0.975	1.028	0.997	3.3	1.4	4.7	5.1
513	0.507	0.063	0.974	1.029	0.997	4.2	1.5	5.7	4.9
522	0.696	0.065	0.975	1.050	0.995	9.8	2.9	12.7	3.4
515	0.696	0.056	0.978	1.060	0.992	9.5	1.4	10.9	-10.9
519	0.898	0.065	0.983	1.060	0.992	11.9	2.1	14.0	-1.7
517	0.898	0.069	0.991	1.060	0.992	5.1	1.5	6.6	4.3

[a] Mole fraction of lighter component.

[b] (A) Correction from the exponential approach to equilibrium.
(B) Correction from the disturbance caused by pumping.
(C) Correction from back diffusion in the capillaries.
(D) Uncertainty from composition analysis.
(E) Uncertainty from temperature measurements.
(F) Total uncertainty.

The least squares expressions for the composition dependences, shown by the solid lines in Figure 31 and obtained using the present data, are given by:

$$1/\alpha_T = -3.94 X_{Ar} + 18.66 \quad \text{for Ar-Kr (4.3\%)}$$
$$1/\alpha_T = -2.44 X_{Ne} + 5.40 \quad \text{for Ne-Kr (4.4\%)}$$
$$1/\alpha_T = -3.82 X_{Ne} + 8.53 \quad \text{for Ne-Ar (3.5\%)}$$

The percentages in parentheses are the average absolute deviations of the experimental points from the least squares equations. The average estimated experimental uncertainties are higher than the average least square deviations for Ar-Kr and Ne-Ar and only slightly lower for Ne-Kr. Therefore, it is fairly safe to infer that the data meet the Laranjeira criteria of demonstrating a linear composition dependence of $1/\alpha_T$ within the experimental uncertainty. The rather large scatter of the data for Ar-Kr is attributed to a smaller separation as compared to the other two systems, which was offset in part by conducting a larger number of experiments. The data of Grew and Wakeham[51] also suffer large scatter for this case, and their four points are not sufficient to determine a reliable composition dependence.

Figure 32 shows the temperature dependence of an equimolar mixture for each of the three systems. The points at 250 K were obtained from the least square equations above and possess a greater statistical weight than the points at higher temperatures. The crosses here again represent the recent low temperature work of Grew and Wakeham.[51] For Ar-Kr, the curves merge in excellent agreement; but for Ne-Ar, the crosses do not form a particularly smooth curve and pass approximately 7% above the open circle at 250 K. Ne-Ar and Ne-Kr thermal diffusion factors have both reached a plateau at 750 K; whereas Ar-Kr is still rising very gradually at this temperature. *(W. L. Taylor)*

Table 14

α_T FOR AN EQUIMOLAR MIXTURE OF Ne-Ar

Run No.	T_{Av} (K)	α_T (Corr.)	Corrections[a] A	B	C	Uncertainties[a] (±%) D	E	F
528	351	0.166	0.990	1.054	0.986	4.6	1.8	6.4
529	450	0.176	0.994	1.041	0.978	6.2	2.2	8.4
535	551	0.173	0.995	1.031	0.970	1.2	3.6	4.8
541	650	0.190	0.996	1.026	0.963	0.9	4.8	5.7
542	750	0.190	0.997	1.021	0.953	8.7	5.2	13.9

α_T FOR AN EQUIMOLAR MIXTURE OF Ne-Kr

527	351	0.273	0.988	1.058	0.988	0.5	5.0	5.5
537	451	0.296	0.994	1.046	0.982	1.1	2.6	3.7
533	551	0.304	0.994	1.036	0.974	0.6	3.1	3.7
539	650	0.307	0.995	1.029	0.967	0.9	5.8	6.7
543	750	0.306	0.996	1.021	0.953	3.3	5.7	9.0

α_T FOR AN EQUIMOLAR MIXTURE OF Ar-Kr

526	351	0.095	0.968	1.056	0.994	4.4	1.8	6.2
531	451	0.118	0.983	1.060	0.990	3.2	1.5	4.7
534	550	0.131	0.990	1.053	0.986	3.5	4.0	7.5
536	550	0.132	0.990	1.053	0.985	1.4	3.3	4.7
540	650	0.145	0.994	1.041	0.978	6.6	4.8	11.4
544	749	0.149	0.996	1.033	0.972	2.6	4.3	6.9

[a] (A) Correction from the exponential approach to equilibrium.
(B) Correction from the disturbance caused by pumping.
(C) Correction from back diffusion in the capillaries.
(D) Uncertainty from composition analysis.
(E) Uncertainty from temperature measurements.
(F) Total uncertainty.

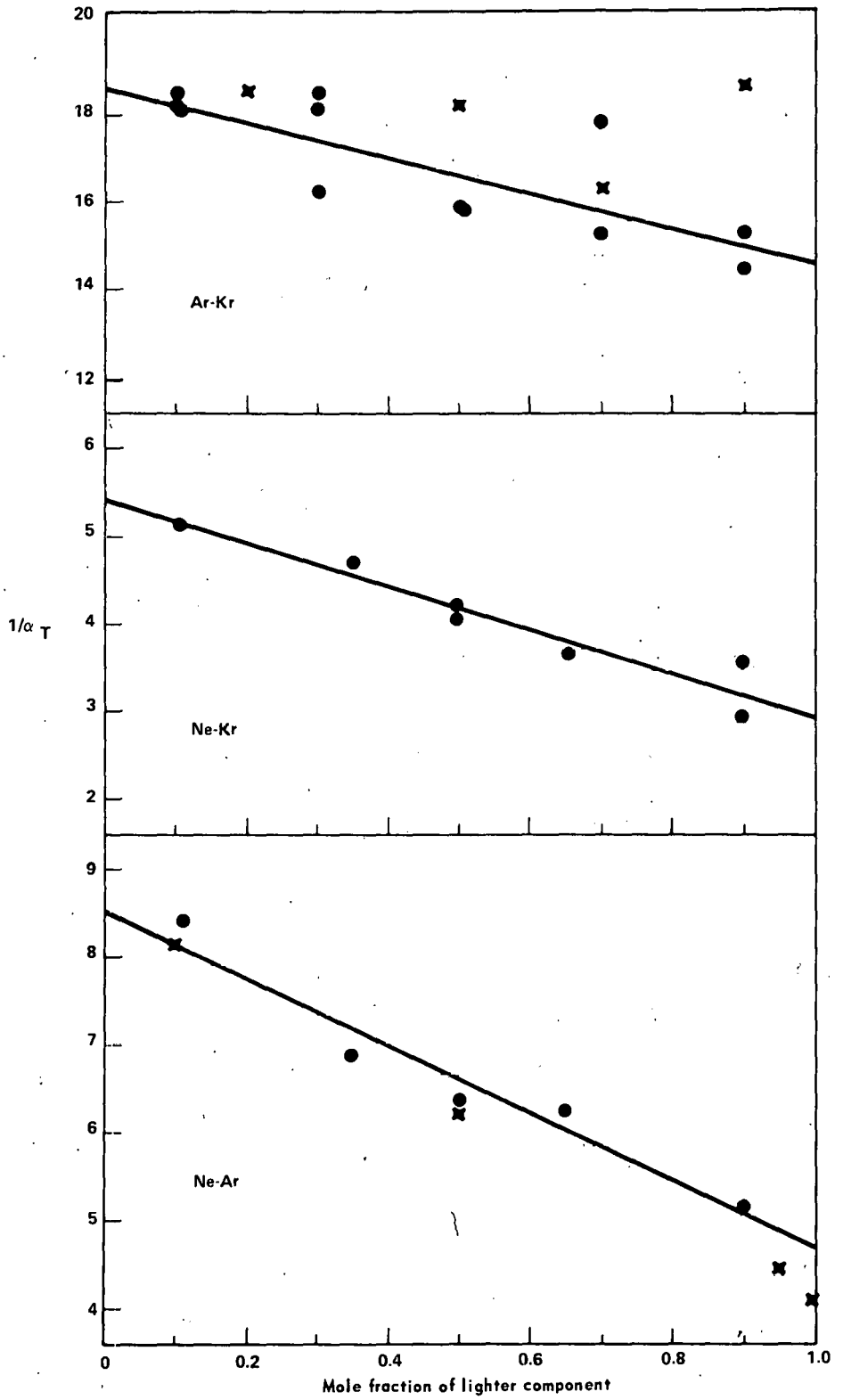

FIGURE 31 - Composition dependence of the reciprocal thermal diffusion factor of Ne-Ar, Ne-Kr, and Ar-Kr mixtures at an average temperature of 250 K. [The experimental points are: ● Present data; and X, Grew and Wakeham (ref 1). The solid line is the least squares fit of the present data to a linear equation].

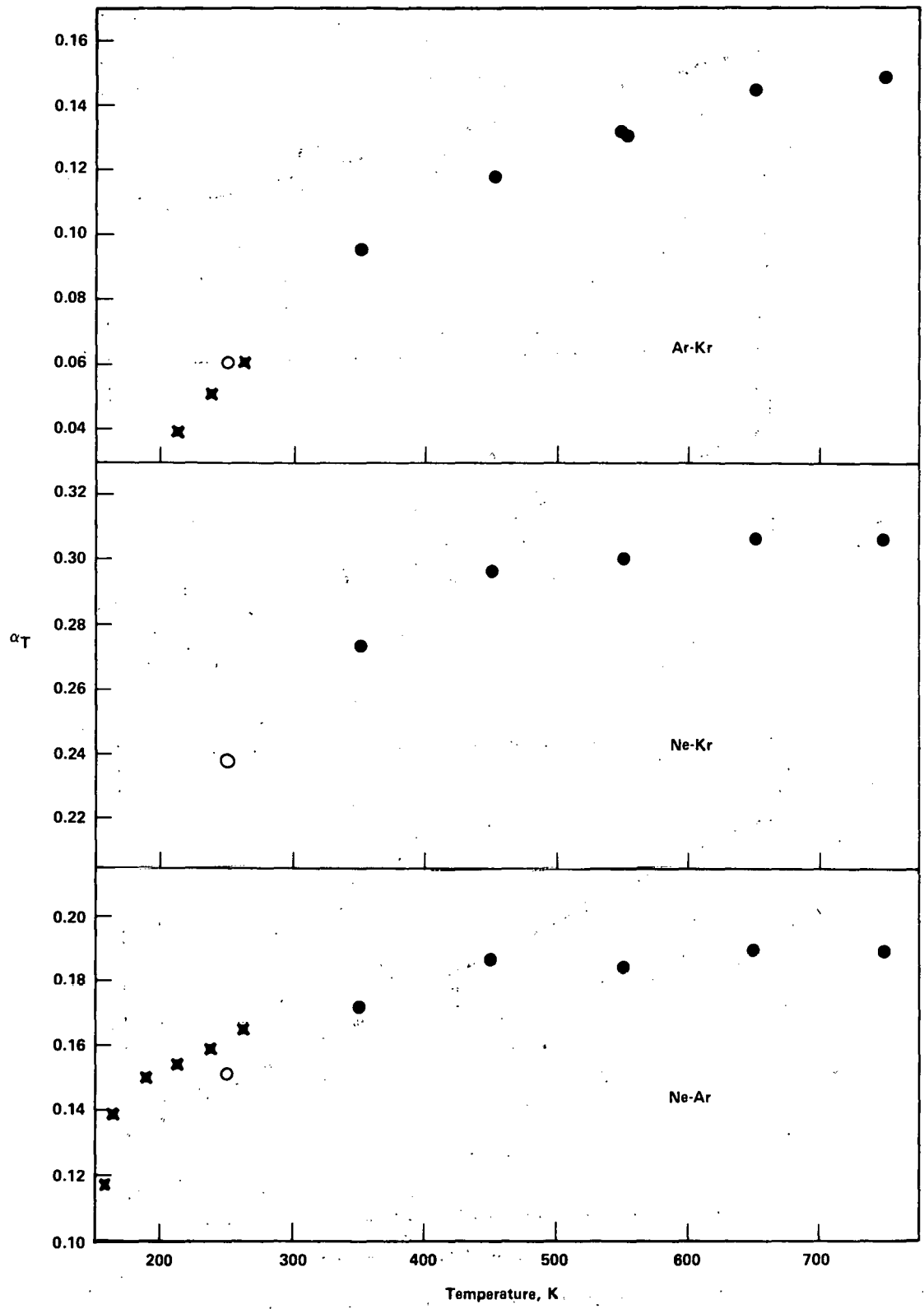

FIGURE 32 - Temperature dependence of the thermal diffusion factor of equimolar mixtures of Ne-Ar, Ne-Kr, and Ar-Kr (The experimental points are the same as above except that the open circles were obtained from the least squares equations given in the text).

References

1. Mound Laboratory Activities for the Division of Physical Research: Jan.-June 1975, MLM-2241 (November 11, 1975), p. 7.

2. D. B. Sullenger et al., Science 163, 955 (1969).

3. B. T. Matthias et al., Science 159, 530 (1965).

4. D. U. Gubser and L. D. Jones, Rept. NRL Prog. (June 1971), pp. 1-14.

5. D. U. Gubser et al., Rept. NRL Prog. (June 1975), pp 1-10.

6. J. Volkl and G. Alefeld, Diffusion in Solids - Recent Developments, A. S. Nowick and J. J. Burton, (eds.), Academic Press, New York, 1975, p. 232.

7. Mound Laboratory Activities for the Division of Physical Research: Jan.-June 1975, MLM-2241 (November 11, 1975) pp. 19-25.

8. A. J. Maeland, J. Phys. Chem., 68, 2197 (1964).

9. S. Kazama and Y. Fukai, Phys. Letters, 51A, 373 (1975).

10. A. C. Switendick, Hydrogen Energy, T. N. Veziroglu, (ed), Plenum Press, New York, 1975, p. 1029.

11. R. M. Cotts, Ber. Bunsenges, Physik. Chem., 76, 760 (1972).

12. A. Schmolz and F. Noack, Ber. Bunsenges, Physik. Chem., 78, 339 (1974).

13. G. K. Schoep, N. J. Poulis, and R. R. Arons, Physica, 75, 297 (1974).

14. Y. Fukai and S. Kazama, Scripta Met., 9, 1073 (1975).

15. H. Asano and M. Hirabayshi, Phys. Status Solidi A: 16, 69 (1973).

16. R. R. Arons, H. G. Bohn, and H. Lutgemeier, J. Phys. Chem. Solids, 35, 207 (1974).

17. C. Korn and D. Zamir, J. Phys. Chem. Solids, 31, 489 (1969).

18. E. A. Bondietti, S. A. Reynolds, and M. H. Shanks, Interaction of Plutonium with Complexing Substances in Soils and Natural Waters, IAEA - SM - 199/51, Publication No. 788, Environmental Sciences Division, ORNL.

19. J. A. Perez-Bustamante, II Oxidation States of the Element, MLM-1747 (TR) (July 10, 1970), 55 pp. [translated from Energia Nuclear (Madrid), 13:57, 23-45 (1969)].

20. G. L. Silver, Dissolution Methods, MLM-2234 (Jan. 6, 1976), 23 pp.

21. G. B. Alexander, Silica and Me, The Career of an Industrial Chemist, Doubleday and Company, Inc., New York, N.Y. 1967, Chapter 6.

22. G. L. Silver, Plutonium in Natural Waters, MLM-1870 (Dec. 16, 1971), 15 pp.

23. Mound Laboratory Activities for the Division of Physical Research: Jan.-June 1974, MLM-2168 (August 30, 1974), pp. 31-35.

24. Mound Laboratory Activities for the Division of Physical Research: July-Dec. 1973, MLM-2118 (February 28, 1974), pp. 32-35.

25. Mound Laboratory Activities for the Division of Physical Research: Jan-June 1975, MLM-2241 (November 11, 1975), pp. 29-31.

26. Mound Laboratory Activities for the Division of Physical Research: July-Dec. 1974, MLM-2198 (April 10, 1975), pp. 38-42.

27. Mound Laboratory Activities for the Division of Physical Research: Jan-June 1975, MLM-2241 (Nov. 11, 1975), pp. 32-36.

28. Y. V. Egorov, "Radiocolloids in Sorption Systems," in Coprecipitation and Adsorption of Radioactive Elements, V. M. Vdovenko (ed.), Israel Program for Scientific Translations, Jerusalem, 1967, p. 130.

29. C. E. Mellish, J. A. Payne, and G. Worrall, Radiochimica Acta, 2:4, 204 (1964).

30. J. B. Andelman and T. C. Rozzell in Radionuclides in the Environment, S. C. Freiling (ed.), Chapter 8, A.C.S. Advances in Chemistry Series No. 93, American Chemical Society, Washington, D.C., 1970

31. F. Kepak, Chemical Reviews, 71:4, (1971).

32. Mound Laboratory Activities for the Division of Physical Research: Jan.-June 1975, MLM-2241 (November 11, 1975), pp. 32-38.

33. Mound Laboratory Activities for the Division of Physical Research: July-Dec. 1974, MLM-2198 (April 10, 1975), pp. 38-42.

34. Chemical Engineering Deskbook - Chemicals, McGraw-Hill, October 8, 1973, p. 61.

35. J. F. Honstead, L. L. Ames, Jr., and J. L. Nelson, "Mineral Reactions - A New Waste Decontamination Process", Health Physics, Vol. 8, 1962, pp. 191-196.

36. J. H. Perry, Chemical Engineer's Handbook, Fourth Edition, McGraw-Hill Book Company, New York, New York, pp. 16-2 to 16-15.

37. Mound Laboratory Activities for the Division of Physical Research: July-Dec. 1972, MLM-2013 (February 14, 1973), pp. 56-59.

38. Mound Laboratory Activities for the Division of Physical Research: Jan.-June 1975, MLM-2241 (November 11, 1975), p. 40.

39. G. L. Silver, Anal. Chem., 41:3, 548 (1969).

40. Mound Laboratory Activities for the Division of Physical Research: July-Dec. 1974, MLM-2198 (April 10, 1975), pp. 43-45.

41. W. M. Rutherford, J. Chem. Phys., 59, 6061 (1973).

42. Mound Laboratory Activities for the Division of Physical Research: Jan.-June 1975, MLM-2241 (November 11, 1975), p. 41.

43. Mound Laboratory Activities for the Division of Physical Research: July-Dec. 1973, MLM-2118 (February 28, 1974), p. 17.

44. Mound Laboratory Activities for the Division of Physical Research: Jan.-June 1975, MLM-2241 (November 11, 1975), p. 47.

45. Mound Laboratory Activities for the Division of Physical Research: July-Dec. 1974, MLM-2198 (April 10, 1975), pp. 52-57.

46. K. Berkling et al., Z. Physik, 166, 406 (1962).

47. J. W. Bredewout, Thesis, Rijksuniversiteit Leiden (Netherlands), 1962.

48. E. W. Rothe and R. H. Neynaber, J. Chem. Phys., 43, 11 (1965).

49a. Stable Gaseous Isotope Separation and Purification: April-June, 1966, MLM-1353 (Feburary 10, 1967), 35 pp.

49b. W. J. Haubach and G. R. Grove, Stable Gaseous Separation and Purification: July-September 1966, MLM-1367 (April 21, 1967), 57 pp.

50. R. J. Munn, E. A. Mason, and F. J. Smith, J. Chem. Phys., 41, 3978 (1964).

51. K. E. Grew and W. A. Wakeham, J. Phys. B:Atom. Molec. Phys., 4, 1548 (1971).

Distribution

External

TID-4500, UC-4 and 22 (169)

W. J. Haubach, Molecular and Geo-Sciences Br., Div. of Physical Research, ERDA
C. P. Sutter/R. N. Diebel, Atlantic Richfield Hanford Company, (ERDA)
F. D. Stevenson, Molecular and Geo-Sciences Br., Div. of Physical Research, ERDA

Consultants

C. F. Curtiss,
University of Wisconsin
C. F. Eck
Miamisburg, Ohio
D. F. Griffing
Miami University (Ohio)
R. E. Miers
Ft. Wayne, Indiana
G. W. Powell
Ohio State University
A. Shapiro
University of Cincinnati
H. F. Swift
University of Dayton Research Institute
D. White
University of Pennsylvania
H. W. Mattson
Monsanto Company

Internal

V. L. Avona
W. T. Cave
R. J. DeSando
C. W. Huntington
B. E. Jepson
L. V. Jones
E. Michaels
W. J. Roos
W. M. Rutherford
R. A. Schwind
G. L. Silver
W. L. Taylor
H. L. Turner
R. E. Vallee
J. G. Villars (2)
E. A. Walker
R. M. Watrous

Document Control
Library (15)
Publications